SYNTHESIS AND DIP-PEN NANOLITHOGRAPHICAL PATTERNING OF FERRITE NANOPARTICLES

by

JINGWEN HE

Presented to the Faculty of the Graduate School of

The University of Texas at Arlington in Partial Fulfillment

of the Requirements

for the Degree of

MASTER OF SCIENCE IN MATERIALS SCIENCE AND ENGINEERING

THE UNIVERSITY OF TEXAS AT ARLINGTON

December 2009

ACKNOWLEDGEMENTS

I sincerely thank Dr. Choong-Un Kim for his support and for being my committee member. I would also like to thank Dr. Fuqiang Liu or reviewing my thesis work and for being my committee member. I express my gratitude to all the professors and the department staff for offering their support whenever required, especially our secretary, Jennifer Standlee for helping me with ordering research supplies and with my academic paperwork.

I would like to say thanks to my supervisor Dr. Yaowu Hao, who gave many valuable suggestions with his rich experience and knowledge. I appreciate the help of Dr. Fatima Z. Amir and Mr. Eduardo Maldonado at NanoFAB who trained me on various equipments. I also would like to thank Dr. Jiechao Jiang for his support in using the characterization equipments at Characterization Center for Materials and Biology.

I appreciate the help of my colleagues and all the friends who motivated and supported me during my thesis work. I express my thanks to Punnapob Punnakitikashem who introduced me to Hao's group and Shih-Hsin Chang who taught me basic lab skills at the very beginning. I thank Chivarat Muangphat and Orathai Thumthan who assisted me with some characterization work for my thesis. I thank Chien-Wen Huang, Yi-Jiun Li, Megha Panuganti, Jie He, Hou-Kuan Lee, Liang-Chien Ma, Hong-Wen Huang and for their consistent support during my entire graduate career.

Finally I devote my heartiest appreciation to my parents, my aunts Miao-Xiang He and Liang-Yan He and my cousin Lulu's family for their love and affection that inspired me throughout my life.

November 24, 2009

ABSTRACT

SYNTHESIS AND DIP-PEN NANOLITHOGRAPHICAL PATTERNING

OF FERRITE NANOPARTICLES

Jingwen He, M.S.

The University of Texas at Arlington, 2009

Supervising Professor: Yaowu Hao

Magnetic nanoparticles are of great interest for researchers from a wide range of disciplines, including magnetic fluids, catalysis, biotechnology/biomedicine, magnetic resonance imaging, data storage, and environmental remediation. Ferrites, a class of ferrimagnetic ceramic compounds with the chemical formula of MFe_2O_4, where M represents any one of several metallic elements such as Mg, Fe, Co, Ni, Cu and so on, are commonly used magnetic materials for nanoparticles. Magnetite (Fe_3O_4) is the prototype of ferrites. Magnetite nanoparticles have been prepared through the co-precipitation of Fe^{2+} and Fe^{3+} aqueous salt solutions by addition of base. They exhibit a size distribution from 4 nm to 16 nm, showing properties of superparamagnetism. Although co-precipitation is an easy and inexpensive method to prepare magnetite nanoparticles, the control of the particle size becomes the biggest experimental challenge. Centrifugation has been employed as a simple way for size selection.

Dip-pen nanolithography (DPN) which was invented in 1999 by Mirkin's group in Northwestern University has been reported as a unique technique with a high resolution for transferring ink molecules on to substrate to create different kinds of micro- or nanostructures. In a typical lithographical experiment, an atomic force microscope (AFM) tip is coated with ink molecules. They are delivered to the surface of a substrate through or over a water meniscus

that forms between the tip and the substrate. Water meniscus works as a medium for ink transportation. The self-assembly of ink molecules deposited using DPN can be modeled as a two dimensional diffusion with a source (AFM tip). Dot- and line- features of magnetite nanoparticles within micro- and nanoscale have been generated on 16-mercaptohexadecanoic acid (MHA) patterns created by DPN, giving a precise control of size and position. Dot diameter can be tuned by adjusting the writing time which has a $t^{1/2}$ dependence (where t is the tip-substrate contact time). Line width has a linear relationship with the scanning speed. The concentration of suspension of magnetite nanoparticles is crucial for the passivating effect of 1-Octadecanethiol (ODT). The optimum value of concentration of the magnetite nanoparticles suspension has been obtained.

TABLE OF CONTENTS

LIST OF ILLUSTRATIONS

LIST OF TABLES

THESIS OVERVIEW

The thesis consists three major chapters: Chapter 1 – Introduction; Chapter 2 – Synthesis and characterization of ferrite nanoparticles; Chapter 3 – Dip-pen nanolithographical patterning of magnetite nanoparticles.

In Chapter 2, a brief introduction of ferrite nanoparticles including ferrite spinel crystal structure and their classification as well as applications has been given. Finite-size effects and synthesis methods including co-precipitation, thermal decomposition, microemulsion and hydrothermal synthesis of magnetite nanoparticles have been reviewed followed by a demonstration of preparation of magnetite nanoparticles ranging from 4nm to 16nm via co-precipitation method. Physical and magnetic properties of magnetite nanoparticles obtained by this method have been characterized by transmission electron microscope (TEM) and vibrating sample magnetometer (VSM) respectively.

In Chapter 3, the technique of dip-pen nanolithography has been described including its diffusion model, tip-substrate combination and comparison of it to other lithographical methods. Different kinds of inks patterned via dip-pen nanolithography (DPN) have been reviewed, followed by a description of overall process of DPN patterning of magnetite nanoparticles. Also discussed include the control of patterned feature (dots and lines) size by adjusting the writing/tip-substrate contact time or the writing/scan speed. Chemical interaction/effects involved in DPN patterning experiment have been studied in order to determine the optimum value of nanoparticles suspension concentration for patterning and passivating the substrate.

CHAPTER 1

INTRODUCTION

For the past decades, nanotechnology which is the understanding and control of matter with structure size on a sub-100nm scale has been developed to such an extent that it has become possible to synthesis, characterize and tailor the functional properties of materials at the nanoscale. A significant aspect of the nanoscale material is that the smaller it gets, the larger its relative surface area becomes. In this case, physical, chemical, thermal, mechanical as well as magnetic properties are no longer the same as bulk materials.

Recently, synthesis of magnetic nanoparticles has been a field of intense study, which is driven by scientific interest and their practical applications. Size effects and the large surface area of magnetic nanoparticles dramatically change their magnetic properties. Magnetic nanoparticles are of great interest for a wide range of applications, including magnetic fluids, catalysis, biotechnology/biomedicine, magnetic resonance imaging, data storage, and environmental remediation.

Ferrites, a class of ferrimagnetic ceramic compounds with the chemical formula of MFe_2O_4, where M represents any one of several metallic elements such as Mg, Fe, Co, Ni, Cu and so on, are commonly used magnetic materials for nanoparticles. Magnetite (Fe_3O_4) is the prototype of ferrites which has an inverse-spinel crystal structure. Magnetite nanoparticles have been prepared through several methods including co-precipitation, thermal decomposition, microemulsion and hydrothermal synthesis methods, among which co-precipitation is the easiest way to obtain a big yield of products. Here, using co-precipitation magnetite nanoparticles have been synthesized and characterized. They exhibit a size distribution from 4 nm to 16 nm, and shown superparamagnetic properties. Although co-precipitation is an easy

and inexpensive method to prepare magnetite nanoparticles, the control of the particle size becomes the biggest experimental challenge. Here, a simple centrifugation method is used to separate ultra-small nanoparticles (< 5 nm).

Dip-pen nanolithography (DPN) which was invented in 1999 by Mirkin's group in Northwestern University has been reported as a unique technique with a high resolution for transferring ink molecules onto the substrate to create different kinds of micro- or nanostructures. DPN is a positive printing mode based on conventional atomic force microscope (AFM). In a typical lithographical experiment, an AFM tip is coated with ink molecules which could be small organic molecules, polymers, DNA, metal ions and so on. They are delivered to the surface of a substrate through or over a water meniscus that forms between the tip and the substrate. Water meniscus works as a medium for ink transportation. The self-assembly of ink molecules deposited using DPN can be modeled as a two dimensional diffusion with a source (AFM tip). DPN is not the only lithographic tool that allows direct transport of molecules from tips to substrates of interest via a positive printing mode. However, if one is trying to selectively write various types of molecules at specific positions within a particular type of nanostructure, DPN would outstand. Also, DPN can be utilized to create templates for the direct assembly of different kinds of particles. Dot- and line- features of magnetite nanoparticles within micro- and nanoscale have been generated on 16-mercaptohexadecanoic acid (MHA) patterns created by DPN, giving a precise control of size and position. Dot diameter can be tuned by adjusting the writing time which has a $t^{1/2}$ dependence (where t is the tip-substrate contact time). Line width has a linear relationship with the scanning speed. The concentration of suspension of magnetite nanoparticles is crucial for the passivating effect of 1-Octadecanethiol (ODT). The optimum value of concentration of the magnetite nanoparticles suspension has been obtained.

CHAPTER 2

SYNTHESIS AND CHARACTERIZATION OF FERRITE NANOPARTICLES

2.1 Ferrite Nanoparticles and Their Applications

Ferrites are a class of ferrimagnetic ceramic compounds with the chemical formula of MFe_2O_4, where M represents any one of several metallic elements such as Mg, Fe, Co, Ni, Cu and so on. The prototype ferrite is Fe_3O_4, the mineral magnetite, sometimes called lodestone. Compared with most other technologically useful magnetic materials such as iron and metallic alloys, ferrites have high permeability and time/temperature stability and can perform much better at high frequencies because they and high electrical resistivity. Ferrites are the best core material choice for frequencies from 10 kHz to a few hundred MHz when one requires the combination of low cost, high Q (inductor quality), high stability and low volume. Another important factor in choosing ferrites is that they are generally cheaper than other magnetic metals and alloys. Moreover, no other magnetic material has magnetic and mechanical parameters as flexible as those of ferrites [1].

2.1.1. Structure of Spinel Ferrites

Ferrites are a class of sipnels, which can be described as a cubic close-packed FCC arrangement of oxygen atoms, with M^{2+} and Fe^{3+} at tetrahedral and octahedral sites (termed as A and B-sites in Figure 2.1, respectively). The spinel structure contains two cation sites for metal cation occupancy. There are 8 tetrahedral sites and 16 octahedral sites.

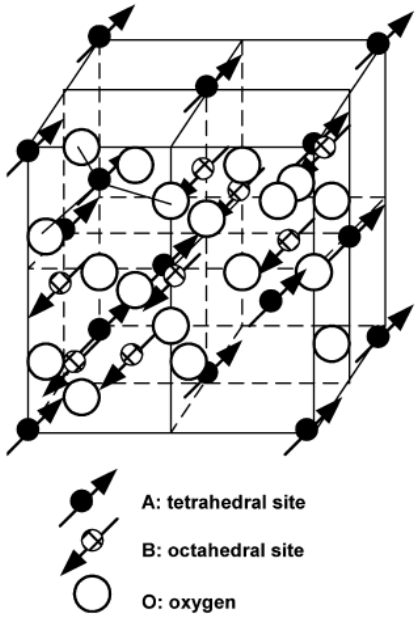

Figure 2.1 Structure of a partial unit cell and ferrimagnetic ordering of spinel ferrite [1].

When the A-sites are occupied by M^{2+} cations and the B-sites are occupied by Fe^{3+} cations, the ferrite is called a normal spinel. Structural formula of such ferrites can be written as $M^{2+}[Fe^{2+}Fe^{3+}]O_4^{2-}$. This kind of distribution takes place in zinc ferrites $Zn^{2+}[Fe^{2+}Fe^{3+}]O_4^{2-}$.

If all A-sites are occupied by Fe^{3+} cations and the B-sites are randomly occupied by M^{2+} and Fe^{3+} cations, the structure is referred to as an inverse spinel. Structural formula of these ferrites is $Fe^{3+}[M^{2+}Fe^{3+}]O_4^{2-}$ or $MO_2 \cdot Fe_2O_3$. Magnetite Fe_3O_4, nickel ferrite $NiFe_2O_4$ and cobalt ferrite $CoFe_2O_4$ have inversed spinel structure.

In mixed spinel structure, cations M^{2+} and Fe^{3+} occupy both A and B-positions; structural formula of this ferrite is $M^{1-\delta\ 2+}Fe^{\delta\ 3+}[M^{\delta\ 2+}Fe^{2-\delta\ 3+}]O_4^{2-}$, where δ is the degree of inversion. $MnFe_2O_4$ represents this type of structure and has an inversion degree of δ = 0.2 and its structural formula therefore is $Mn^{0.8\ 2}+Fe^{0.2\ 3+}[Mn^{0.2\ 2+}Fe^{1.8\ 3+}]O_4^{2-}$. Mn–Zn ferrites also have a mixed spinel structure (Zn^{2+} prefers to occupy A-sites) $Zn^{x\ 2+}Mn^{y\ 2+}Fe^{1-x-y\ 3+}[Mn^{1-x-y\ 2+}Fe^{1+x+y\ 3+}]O_4^{2-}$, where δ =1−x−y.

Magnetically, spinel ferrites display ferrimagnetic ordering. The magnetic moments of cations in the A and B-sites are aligned parallel with respect to one another. Between the A and B-sites the arrangement is antiparallel and as there are twice as many B-sites as A-sites, there is a net moment of spins yielding ferrimagnetic ordering for the crystal. The choice of metal cation and the distribution of ions between the A and B-sites therefore, offer a tunable magnetic system [2].

Magnetic properties of ferrites have been explained by Neel [5], who postulated that magnetic moments of ferrites are a sum of magnetic moments of individual sublattices. In spinel ferrites, sublattice α consisting of cations in tetrahedral positions and sublattice β with cations in octahedral positions. Exchange interaction between electrons of ions in these sublattices has different value. Usually interaction between magnetic ions of sublattices α and β (α–β interaction) is the strongest. α–α interaction is almost ten times weaker and β–β interaction is the weakest. The dominant α–β interaction leads to a complete or partial antiferromagnetism (ferrimagnetism) [3].

The arrangement of spin moments can be illustrated with magnetite (Fe_3O_4 or $FeO_2{\cdot}Fe_2O_3$), the most common ferrite which has an inverse spinel structure. Within this inverse spinel structure, half the trivalent (Fe^{3+}) ions are situated in octahedral sites, the other half, in tetrahedral sites. The divalent (Fe^{2+}) ions are all located in octahedral positions. As seen in Table 2.1, the spin moments of all the Fe^{3+} ions in the octahedral positions are aligned parallel to one another; however, they are directed oppositely to the Fe^{3+} ions disposed in the tetrahedral positions, which are also aligned. This results from the antiparallel coupling of adjacent iron ions. Thus, the spin moments of all Fe^{3+} ions cancel one another and make no net contributions to the magnetization of the solid. All the Fe^{2+} ions have their moments aligned in the same direction, which total moment is responsible for the net magnetization. Thus, the saturation magnetization of a ferrimagnetic solid may be computed from the product of the net

spin magnetic moment for each Fe^{2+} ion and the number of Fe^{2+} ions; this would correspond to the mutual alignment of all the Fe^{2+} ion magnetic moments in the Fe_3O_4 specimen [1].

Table 2.1 the Distribution of Spin Magnetic Moments for Fe^{2+} and Fe^{3+} Ions in a Unit Cell of Fe_3O_4 [1].

Cation	Octahedral Lattice Site	Tetrahedral Lattice Site	Net Magnetic Moment
Fe^{3+}	↑ ↑ ↑ ↑	↓ ↓ ↓ ↓	Complete Cancellation
	↑ ↑ ↑ ↑	↓ ↓ ↓ ↓	
Fe^{2+}	↑ ↑ ↑ ↑	—	↑ ↑ ↑ ↑
	↑ ↑ ↑ ↑		↑ ↑ ↑ ↑

Again, from the spinel ferrite chemical formula, MFe_2O_4 or $MO_2 \cdot Fe_2O_3$, in addition to Fe^{2+}, M^{2+} may represent other divalent ions such as Ni^{2+}, Mn^{2+}, Co^{2+}, and Cu^{2+}, each of which possesses a net spin magnetic moment different from 4; several are listed in Table 2.2. Thus, by adjusting the composition, ferrite compounds with certain range of magnetic properties may be produced. For example, nickel ferrite has the formula $NiFe_2O_4$, with Fe^{3+} occupying all octahedral sites and half of the tetrahedral sites. The remaining tetrahedral sites in the spinel are occupied by Ni^{2+}. Other compounds may also be produced containing mixtures of two divalent metal ions such as (Mn, Mg) Fe_2O_4, in which the Mn2+: Mg^{2+} ratio may be varied (called mixed ferrites) [1].

Table 2.2: Net Magnetic Moments for Six Cations .

Cation	Net Spin Magnetic Moment (Bohr magnetons)
Fe^{3+}	5
Fe^{2+}	4
Co^{2+}	3
Ni^{2+}	2
Cu^{2+}	1
Mn^{2+}	5

2.1.2. Classification and Applications of Spinel Ferrites

Magnetic materials can be grouped into two types, soft and hard. This is the classification based on their ability to be magnetized and demagnetized. Soft materials are easy to magnetize and demagnetize, so are used for electromagnets, while hard materials are used for permanent magnets. They can also be classified based on their coercive field strength into soft and hard materials. With soft magnetic materials the hysteresis loop is small (low coercive field strength, independent of magnetic field amplitude); with permanent magnets however it is large (high coercive field strength). Table 2.3 gives a comparative account of both types [4].

Table 2.3 the Comparative Properties of Soft and Hard Magnetic Materials [4].

Soft magnetic	Hard magnetic
High saturation magnetization (1–2T)	High saturation magnetization (0.3–1.6T)
Low coercivity (H_c)	High coercivity
High permeability	Not important, but low
Low anisotropy	High anisotropy
Low magnetostriction	Not important
High Curie temperature (T_c)	High T_c
Low losses	High-energy product
High electrical resistivity	Not important

The general properties and applications of hard and soft magnetic materials are given in Table 2.4 [1].

Table 2.4 Properties and Applications of Hard and Soft Magnetic Materials [1].

Material	General properties and application
(a) Hard magnetic materials	
Aluminium–nickel–cobalt alloy (ALNICO), sometimes with copper and titanium	Magnets can be cast into complex shapes and perform well at high temperatures Used in applications such as instruments and meters that requires very stable temperature properties like electronic ignition systems, generators, vending machines, etc.
Rare-earth alloys (samarium)	High magnetic strength Used in wrist watches and medical implants
Neodymium–iron–boron alloys	Very low magnetic strength Used in low weight requirement applications
Hard ferrite–barium and strontium ferrite	Low cost Widespread use, including electronic applications
(b) Soft magnetic materials	
Iron with 3–4% silicon	AC motors, generators and transformers
Metallic glass-combinations of Fe, Co, Ni, B and Si	Low energy loss Use in power transformers, magnetic sensors and recording equipment
Nickel–iron alloys	Low permeability applications Used in telecommunications, aeronautical, aerospace engineering, cryogenic engineering (liquefied natural gas tankers), etc.
Hard ferrite–iron, nickel and cobalt ferrite	Low electrical conductivity reduces eddy current losses Used in high-frequency applications

2.2 Background Introduction and Literature Review

2.2.1. Different Kinds of Magnetism and Hysteresis Loop

Materials behave differently to an externally applied magnetic field. According to their response, materials can be classified into five basic types of magnetism: diamagnetism, paramagnetism, ferromagnetism, antiferromagnetism and ferrimagnetism. Descriptions of orientations of the magnetic moments in a material help to identify different forms of magnetism observed in nature. Figure 2.2 illustrates schematically the configurations of magnetic dipole moments for materials with different magnetism when there is no applied field [5].

For diamagnetic materials, in the presence of an externally applied magnetic field, the atomic current loops created by the orbital motion of the electrons respond to oppose the applied field. Diamagnetism is found in all materials; however, since it is so weak it can be observed only when other types of magnetism are totally absent. This form of magnetism is of magnetism is of little practical importance.

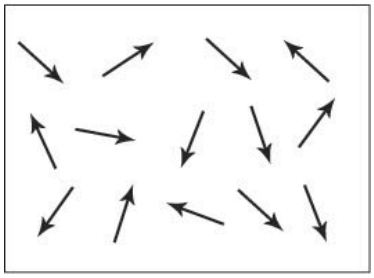

(a)

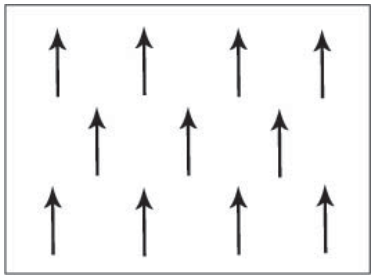

(b)

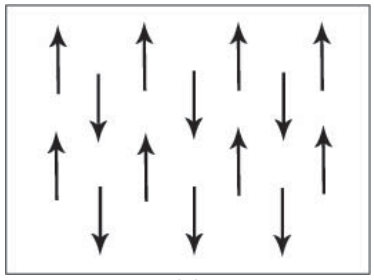

(c)

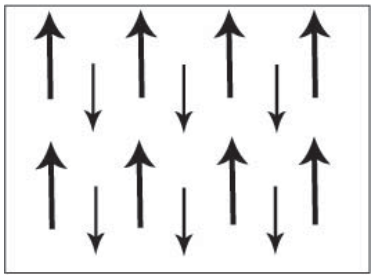

(d)

Figure 2.2 Schematically Show Alignment of Magnetic Moments without Externally Applied Magnetic Field in (a) Paramagnetic, (b) Ferromagnetic, (c) Antiferromagnetic and (d) Ferrimagnetic Materials [5].

In paramagnetic materials, when there is no magnetic field, the magnetic moments tend to be randomly orientated due to thermal fluctuations (Figure 2.2 (a)). In an applied magnetic field these moments start to align parallel to the field such that the magnetization of the material is proportional to the applied field.

In a ferromagnet, exchange coupling makes the magnetic moments to become aligned parallel to each other (Figure 2.2 (b)). If an external magnetic field of strength H is applied to a ferromagnet of magnetic strength M, the magnetization curve of Figure 2.3 is obtained showing that M increases with H until a saturation value M_S is reached. The magnetization curve displays a hysteresis loop, because domains do not return to their original states when H is decreased after the saturation magnetization value is attained. Thus, when H returns to zero, there is a remnant magnetization M_R which can only be removed by applying a coercive field H_C in the opposite direction to the initially applied field.

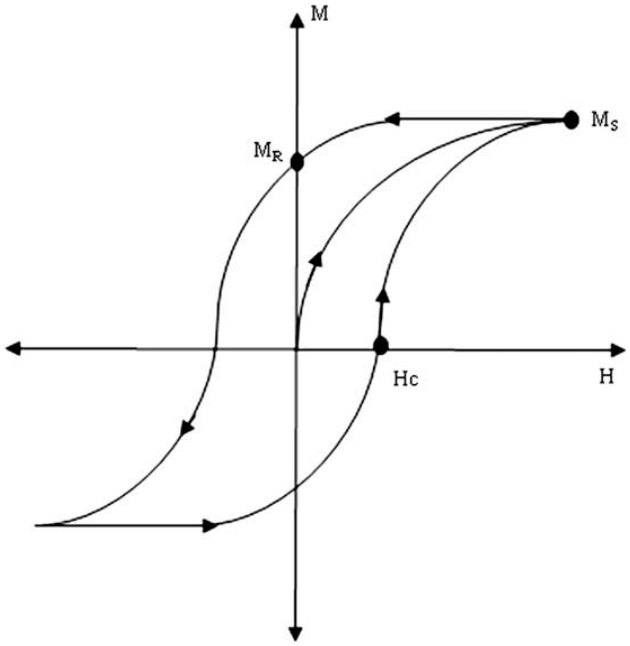

Figure 2.3 Hysteresis Loop of Ferromagnet

For antiferromagnetic materials, magnetic coupling between adjacent atoms or ions results in an antiparallel alignment; the alignment of the moment of neighboring atoms or ions is in exactly opposite directions. In the simplest case (Figure 2.2 (c)), adjacent magnetic moments are equal in magnitude and opposite therefore there is no overall magnetization.

The macroscopic magnetic characteristics of ferrimagnets are similar with those of ferromagnets. The distinction lies in the source of the net magnetic moment. In a ferrimagnet, the aligned magnetic moments are not of the same size; in other words, there is more than one type of magnetic ion. An overall magnetization is produced but not all the magnetic moments may give a positive contribution to the overall magnetization (Figure 2.2 (d)).

2.2.2. Finite-size Effects of Magnetic Nanoparticles

Two key issues of finite-size effects of magnetic nanoparticles are the single-domain limit and the superparamagnetic limit [6]. Herein, these two limits will be discussed respectively.

2.2.2.1 Single-domain

Domains, regions of a ferromagnetic material in which the magnetic dipole moments are aligned parallel, are separated by domain walls. Each domain has its own magnetization vector arising from an alignment of atomic magnetic moments within the domain. The magnetization vectors of all the domains in the material may not be aligned, leading to a decrease in the overall magnetization (Figure 2.4) [7].

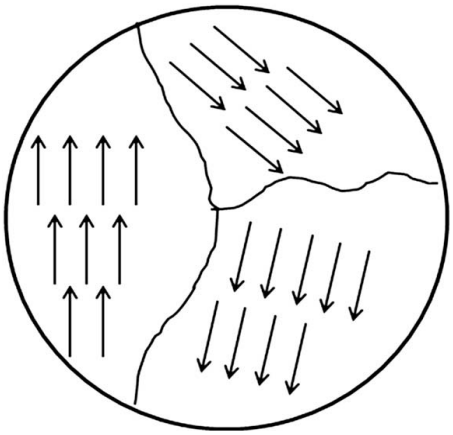

Figure 2.4 Magnetic Domains in a Bulk Material [7].

The formation of the domain walls is a process driven by the balance between the magnetostatic energy (ΔE_{ms}), which increases proportionally to the volume of the materials and the domain-wall energy (E_{dw}), which increases proportionally to the interfacial area between domains. When the sample size becomes smaller, there is a critical volume below which it costs less energy to support the external magnetostatic energy of the single-domain state than to create a domain wall [6]. This critical diameter typically lies in the range of a few tens of nanometers and depends on the material. It is influenced by the contribution from various anisotropy energy terms.

The critical diameter of a spherical particle, D_c, below which it exists in a single-domain state is reached when $\Delta E_{ms}=E_{dw}$, which implies $D_c \approx 18(AK_{eff})^{1/2}/(\mu_0 M^2)$, where A is the exchange constant, K_{eff} is anisotropy constant, μ_0 is the vacuum permeability, and M is the saturation magnetization. Typical values of D_c for some important magnetic materials are listed in Table 2.5 [8].

Table 2.5 Estimated Single Domain Size for Different Special Particles [8].

Material	Dc (nm)
Co (FCC)	7
Co (HCP)	15
Fe	15
Ni	55
Fe_3O_4	128

2.2.2.2 Superparamagnetism

Size reduction in magnetic materials results in the formation of single-domain particles. Further reduction of the size gives rise to the phenomenon of superparamagnetism. Briefly, superparamagnetism occurs when thermal fluctuations or an applied field can easily move the magnetic moments of the nanoparticle away from the easy axis, the preferred crystallographic axes for the magnetic moment to point along. Each particle behaves like a paramagnetic atom, but with a large magnetic moment, because there is still a well-defined magnetic order in each nanoparticle [9].

Superparamagnetism can be understood by considering the behavior of a single-domain particle which is well isolated. The magnetic anisotropy energy for each particle responsible for holding the magnetic moments along a certain direction can be expressed as: $E(\theta)=K_{eff}V\sin^2\theta$, where V is the volume of particle, K_{eff} is anisotropy constant and θ is the angle between the magnetization and the easy axis.

The energy barrier $K_{eff}V$ separates the two energetically equivalent easy directions of magnetization. When the particle size decreases, the thermal energy, k_BT, exceeds the energy barrier $K_{eff}V$ and the magnetization is easily tuned over (Figure 2.5). Under the condition of $k_BT>$

$K_{eff}V$, the system behaves like a paramagnet, instead of atomic magnetic moments, there is now a giant (super) moment inside each particle [10].

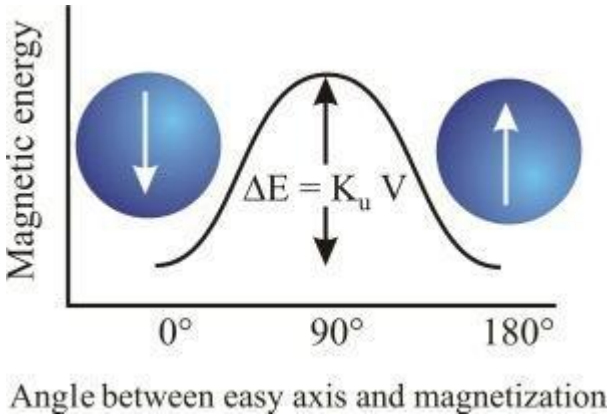

Figure 2.5 Energy Curve for Single Domain Particle [11].

The relaxation time of the particle magnetic moment, t, is given by the Néel-Brown expression Eq. (1) [12], where k_B is the Boltzmann's constant, and $t_0 \approx 10^{-9}$s.

$$t = t_0 \exp (K_{eff}V/k_BT) \qquad \text{Eq. (1) [12]}$$

If the particle magnetic moment reverses at times shorter than the experimental time scales, the system is in a superparamagnetic state, if not, it is in the so-called blocked state. The temperature, which separates these two states, the so-called blocking temperature, T_B, can be calculated by considering the time window of the measurement.

According to Eq. (1) above, it is clear that the blocking temperature, T_B, depends on the effective anisotropy constant, the size of the particles, the applied magnetic field, and the experimental measuring time.

2.2.3. Synthetic Methods of Magnetic Nanoparticles

In the last decades, much research has been devoted to the synthesis of magnetic nanoparticles and a number of methods have been developed to synthesize ferrite nanoparticles, which are among most important magnetic materials, such as Fe_3O_4 [13-15], $MgFe_2O_4$, $MnFe_2O_4$ and $CoFe_2O_4$ [16-17], etc. During last few years, research has been

focused on the control of size, size distribution, shape, crystal structure and surface structure of nanoparticles and their magnetic properties. Several popular methods including co-precipitation, thermal decomposition and/or reduction, micelle synthesis and hydrothermal methods can all be directed at the synthesis of high-quality magnetic nanoparticles.

2.2.3.1 Co-precipitation

Liquid phase methods are generally inexpensive and offer better yields of products as well as ease of surface treatment [18]. Most nanoparticles prepared to date by such methods have been via coprecipitation from aqueous solutions, although other liquid solvents can also be used.

Co-precipitation is a facile and convenient way to synthesize ferrite nanoparticles. Magnetite (Fe_3O_4) nanoparticles can be obtained from aqueous Fe^{2+}/Fe^{3+} salt solutions by adding a base under inert atmosphere at room temperature or at elevated temperature. The phase, size, shape and composition of the magnetic particles depend very much on the type of salts used (e.g. chlorides, sulfates, nitrates), the Fe^{2+}/Fe^{3+} ratio, the reaction temperature, the pH value and ionic strength of the media [19-25]. Once the synthetic conditions are fixed in co-precipitation method, the quality of the magnetite nanoparticles is quite reproducible.

The experimental challenge in the synthesis of Fe_3O_4 by co-precipitation lies in the control of particle size so that a narrow particle size distribution can be achieved. We all know that the blocking temperature depends on particle size, and a wide particle size distribution will result in a wide range of blocking temperatures, therefore non-ideal magnetic behavior for many applications. Particles prepared by co-precipitation unfortunately tend to be rather polydisperse.

Due to the large surface-area to volume ratio, nanoparticles formed by liquid phase coprecipitation tend to aggregate in solution in order to reduce their surface energy [22]. The suspension of nanoparticles can be stabilized by adding anionic surfactants as dispersing agents [26-27]. For example, magnetite nanoparticles with sizes of 4–10 nm can be stabilized in an aqueous solution of 1 wt% polyvinlyalcohol (PVA). However, when using PVA containing 0.1

mol% carboxyl groups as the stabilizing agent, magnetite nanoparticles precipitate in the form of chainlike clusters [28]. This result indicates that the selection of a proper surfactant is an important issue for the stabilization of such particles. Shimoiizaka et al prepared water-based magnetic fluids by dispersing magnetite particles in water containing oleic acid as stabilizing agent [29]. Following this work, Khalafalla and Reimers produced stable aqueous magnetic fluids by using dodecanoic acid as a dispersing agent [29]. The use of saturated and unsaturated fatty acids to stabilize magnetic fluids has been investigated by Wooding et al. [30].

2.2.3.2 Thermal Decomposition

High quality monodisperse and monocrystalline magnetic nanoparticles with controlled size and shape can be produced by the thermal decomposition of organometallic compounds in high-boiling organic solvents containing stabilizing surfactants [31-32] such as oleylamine [32-33], oleic acid [34-35] and steric acid [18]. In principle, the ratios of the starting reagents including organometallic compounds, surfactant, and solvent are the decisive parameters for the control of the size and morphology of magnetic nanoparticles. Also, the reaction temperature, reaction time, as well as aging period may be crucial for the precise control of size and morphology.

Nearly monodisperse Fe_3O_4 nanocrystals, with size adjustable over a 3 to 50nm range could be synthesized [6]. High quality magnetite nanoparticles with diameters ranging from 3 to 20 nm were synthesized via thermal decomposition of Fe (III) acetylacetonate in phenyl/benzyl ether and 2-pyrrolidone [15, 32, 36]. Sun and co-workers have reported the synthesis of monodisperse iron oxide nanoparticles by the thermal decomposition of iron acetylacetonate [32]. They further proposed a simple method to transform hydrophobic nanoparticles into hydrophilic ones by adding bipolar surfactants and produced 4 nm magnetite nanoparticles by decomposition of Fe(III) acetylacetonate in a mixture of phenyl ether, 1,2-hexadecanediol, oleic acid, and oleylamine [15, 36].

These results show the possibility and effectiveness of the thermal decomposition method for the synthesis of ferrite magnetic nanoparticles. However, the presence of residual surfactants may hamper the efficiency of subsequent surface modification of the synthesized nanoparticles. Additionally, the use of toxic solvents and surfactants may become an issue when taking biocompatibility of the product into account [18, 37].

2.2.3.3 Microemulsion

Microemulsions with water-in-oil two phases consist of nanosized aqueous phase dispersed as microdroplets (typically 1-50nm) in an oil phase and stabilized by surfactant molecules at the water/oil interface have been widely used to obtain iron oxide nanoparticles [38-41]. The surfactant-covered water drops offer a unique microenvironment for the formation of nanoparticles and for limiting their growth. The size of the microemulsion droplets is determined by the water to surfactant ratio. However, the eventual size of the nanoparticles may also be influenced by parameters such as concentration of reactants (especially surfactant) and flexibility of the surfactant film [38].

Spinel ferrite nanoparticles can be synthesized by using microemulsion technique. $MnFe_2O_4$ nanoparticles with controllable sizes from about 4–15 nm are synthesized through the formation of water-in-toluene inverse micelles with sodium dodecylbenzenesulfonate (NaDBS) as surfactant [44]; A cobalt ferrite fluid was reported to be prepared by the reaction of methylamine and in-situ formed cobalt and iron dodecyl sulfate which were made by mixing an aqueous solution of sodium dodecyl sulfate either with iron chloride or with cobalt acetate solution [45]. The size of the cobalt ferrite particles decreases with the decrease of total reactant concentration and the increase of sodium dodecyl sulfate concentration.

Although many types of magnetic nanoparticles have been synthesized using microemulsion method, the particle size and shapes could not be well controlled and usually vary over a relative wide range [6]. Moreover, the yield of nanoparticles is low compared to other methods, such as coprecipitation and thermal decomposition. Since large amounts of

solvent are necessary to yield appreciable amounts of materials, the adverse effects of residual surfactant on the properties of the particles tend to be another disadvantage of this method.

2.2.3.4 Hydrothermal Synthesis

High pressure hydrothermal methods rely on the ability of water at elevated pressures and temperatures to hydrolyze and dehydrate metal salts, and the very low solubility of the resulting metal oxides in water at these conditions to generate supersaturation [42]. The elevated temperatures favor high dehydration rates, as does the high diffusivity of reactants in water at these conditions [43-44]. Very high supersaturations can be achieved in this process because of the very low solubility of metal hydroxides and oxides, so that very fine crystals are obtained [44-47].

A generalized hydrothermal method for synthesizing a variety of different nanocrystals by a liquid–solid–solution reaction has been reported by Li et al. The system consists of metal an ethanol– linoleic acid (liquid), linoleate (solid), and a water–ethanol (solution) at different reaction temperatures under hydrothermal condition s [48]. This synthesis method is based on a general phase transfer and separation mechanism which occurs at the interfaces of the liquid, solid, and solution phases present during the synthesis. As an example, Fe_3O_4 and $CoFe_2O_4$ nanoparticles can be prepared in very uniform sizes of about 9 and 12 nm [49].

Key factors such as pressure, temperature, reaction time are all crucial to maintain high nucleation rates and to control growth [50-51]. The process is environmentally friendly and versatile, since it does not involve any organic solvents or post-treatments such as calcination [52].

2.2.3.5 Comparison of Four Synthetic Methods

The advantages and disadvantages of the four above discussed synthetic methods are briefly summarized as in Table 2.6 [6].

Table 2.6 Summary Comparison of Four Synthetic Methods [6].

Synthetic method	Synthesis	Reaction temp. [°C]	Reaction period	Solvent	Surface-capping agents	Size distribution	Shape control	Yield
co-precipitation	very simple, ambient conditions	20–90	minutes	water	needed, added during or after reaction	relatively narrow	not good	high/ scalable
thermal decomposition	complicated, inert atmosphere	100–320	hours–days	organic compound	needed, added during reaction	very narrow	very good	high/ scalable
microemulsion	complicated, ambient conditions	20–50	hours	organic compound	needed, added during reaction	relatively narrow	good	low
hydrothermal synthesis	simple, high pressure	220	hours ca. days	water-ethanol	needed, added during reaction	very narrow	very good	medium

Coprecipitation is the simplest method with a high yield of production. In terms of size and morphology control of the nanoparticles, thermal decomposition is the preferred method developed to date. Microemulsion methods can also be used to create monodispersed nanoparticles with various morphologies as an alternative. However, large amount of solvent is required in this method, which becomes the biggest drawback of it. Hydrothermal synthesis is a method with relatively little exploration although it also allows the creation of high-quality nanoparticles. To date, magnetic nanoparticles prepared by using coprecipitation and thermal decomposition methods are best studied, and most widely used. Another good thing is that they can be done on a large scale.

2.2.4. Applications of Magnetic Nanoparticles

The magnetic properties of magnetic nanoparticles have been in good interest and exploited in a broad range of applications including magnetic inks and seals, catalysts [53-54], as well as in biotechnology or biomedicine [55-57]. These applications demand nanomaterials of specific sizes, shapes, surface characteristics, and magnetic properties.

The use of magnetite in ferrofluids was originally proposed for high-performance seals in space applications. Ferrofluids contain superparamagnetic particles in nanoscale dispersed in aqueous or organic media [58]. A ferrofluid has no net magnetic moment except when it is

under the influence of an applied field. An external magnet is therefore able to trap the fluid in a specific location to act as a seal. Ferrofluids have interesting properties such as magnetic field dependent optical anisotropy that could prove useful in optical switches and tunable diffraction gratings. They are currently employed in sealing computer disk units, and in vibrating environments in place of conventional seals [59].

Magnetic nanoparticles with core–shell structure may enable the development of a new type of catalyst. The shell consists of the catalytically active species, and the magnetic core can act as anchor to separate and recycle the catalyst [7].

Magnetite and maghemite have attracted attention in biomedical applications because of their biocompatibility and low toxicity in the human body [60-61]. A major area of application has been the field of bio-assays where the magnetic properties have been exploited in vitro to manipulate magnetite nanoparticles with an external magnetic field [18, 62]. Wang and co-workers [63] have developed extremely sensitive magnetic microarrays using ferromagnetic sensors to detect binding of target DNA and proteins.

Bio-applications usually require particles that exhibit superparamagnetic behavior at room temperature. Remnant magnetization could lead to agglomeration of these particles, and this must obviously be avoided within the body to prevent blockage of blood vessels. In addition, applications in biology and medical diagnosis require stable magnetic particles in water at neutral pH and physiological conditions [54, 59]. Magnetite or maghemite are by far the most commonly employed materials for biomedical applications [18, 54]. A very promising application of magnetite nanoparticles is in drug delivery as drug carriers. Functionalized superparamagnetic magnetite and maghemite nanoparticles, in combination with an external magnetic field, allow delivery of drugs to the desired target where the medication can be released locally [64-65]. This allows the dosage of the medication to be reduced and any adverse effect of the drugs to be kept to a minimum [64]. The surfaces of nanoparticles used in

drug delivery are generally functionalized with drugs, proteins, and genetic materials to achieve localized delivery of these therapeutic agents [65-66].

Another application of magnetic nanoparticles is hyperthermia in cancer therapy. When a magnetic fluid is exposed to an alternating magnetic field the particles become powerful heat sources, destroying tumor cells since these cells are more sensitive to temperatures in excess of 41℃ than their normal counterparts [65]. The amount of heat generated by magnetic nanoparticles depends strongly on the structural properties of the particles (e.g., size, shape) and should be as high as possible to reduce the dose to a minimum level [10].

2.3 Magnetite Nanoparticles

In this section, the synthesis procedures of ferrite nanoparticles including magnetite and copper ferrite nanoparticles will be introduced. Also, the various characterization techniques used will be provided.

2.3.1. Experimental Procedures

Magnetite (Fe_3O_4) nanoparticles were prepared through the co-precipitation of Fe^{2+} and Fe^{3+} aqueous salt solutions by addition of base [67].

All chemicals were of reagent grade and were used without further purification. Ferric chloride ($FeCl_3$, anhydrous), ferrous chloride tetrahydrate ($FeCl_2 \cdot 4H_2O$, 99+%) , ammonium hydroxide (NH_4OH 28-30wt.% solution of NH_3 in water) and tetramethylammoniu hydroxide ($(CH_3)_4NOH$, 25% certified) were all obtained from Fisher Scientific while HCl (32%) from Sigma Aldrich. 2M HCl were prepared by adding 37.5ml 32% HCl into 150ml DI water.

For preparation of magnetite particles, dissolve 2 g $FeCl_2 \cdot 4H_2O$ in 2.5 ml 2 M HCl solution and 1.6 g $FeCl_3$ in 10 ml 2 M HCl solution at room temperature. Combine ferrous chloride and ferric chloride aqueous solutions in a beaker with a magnetic stirring bar placed in it. Stir vigorously for 30 min, at the same time, 15 ml ammonium hydroxide (NH_4OH 28-30 wt.% solution of NH_3 in water) solution was added dropwise into the beaker by using a transfer pipette, resulting in the immediate formation of a black color precipitate (magnetite, Fe_3O_4).

Continue stirring for 15 min after adding ammonia hydroxide solution. Stop stirring and a strong magnet was used to settle the black precipitate. Most of the liquid was then decanted and disposed of. The remaining solution was stirred further. The solution was centrifuged for 2 min at the speed of 1800 rpm and the supernatant was decanted. Centrifuging step was repeated five times in order to remove the excess ammonia and afford the magnetite particles (Fe_3O_4) [68].

The chemical reactions of Fe_3O_4 precipitation is given in Figure 2.6. The overall reaction could be written as follows [69-70].

$$Fe^{2+} + 2Fe^{3+} + 8OH^- \rightarrow Fe_3O_4 + 4H_2O \quad (1)$$

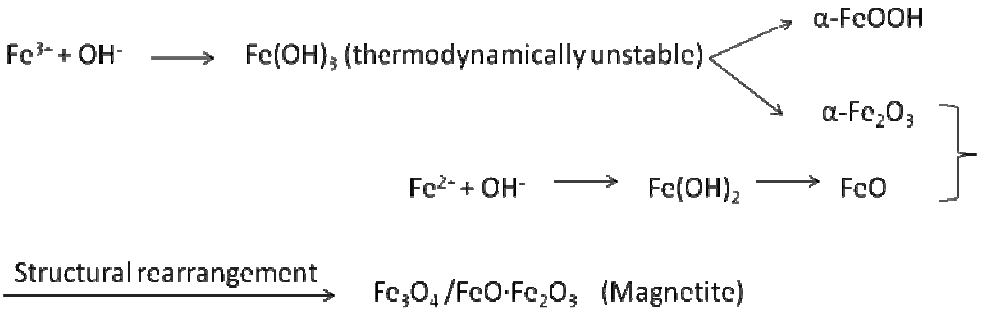

Figure 2.6 Scheme showing the reaction mechanism of magnetite particle formation from an ferrous and ferric chloride aqueous mixture with addition of a base. The precipitate is black in color.

According to the thermodynamics of this reaction, a complete precipitation of Fe_3O_4 should be maintaining a molar ratio of Fe^{3+}:Fe^{2+} = 2:1 under a non-oxidizing oxygen-free environment, while precipitation should be expected to have a PH ranging from 9 to 14. Otherwise, Fe_3O_4 might also be oxidized as

$$Fe_3O_4 + 0.25O_2 + 4.5H_2O \rightarrow 3Fe(OH)_3 \quad (2)$$

This would actually affect the physical and chemical properties of the magnetic nanoparticles. In order to prevent them from possible oxidation in air as well as from aggregation, magnetite nanoparticles produced by reaction (1) are usually coated with organic or inorganic surfactant during or after the precipitation process [71]. For example, magnetite

nanoparticles with sizes of 4-10 nm can be stabilized in an aqueous solution of 1 wt. -% polyvinlyalcohol (PVA). However, when using PVA containing 0.1 mol% carboxyl groups as the stabilizing agent, magnetite nanoparticles in the form of chainlike clusters precipitate. This result indicates that the selection of a proper surfactant is an important issue for the stabilization of such particles.

Taking the stabilization purpose and subsequent application of magnetite nanoparticles in "dip-pen nanolithography" into consideration, the particles obtained via co-precipitation method were then mixed with 10 ml solution of tetramethylammonium hydroxide ($(CH_3)_4NOH$, 25wt.-% solution in water), which was used as a surfactant to prevent aggregations of particles in a aqueous environment as well as to make the magnetite particles positively charged so that their affinity for negatively charged surface (MHA SAMs for example) would be increased. Figure 2.7 indicates the repulsive double-layer interaction stabilization of magnetite particles coated with tetramethylammonium hydroxide. As shown in the figure, hydroxide part of the surfactant has good affinity to magnetite, leaving the ammonium part pointing out. The repulsion between particles makes the suspension stabilized. On the other hand, a positively charged surface around the particles could be created.

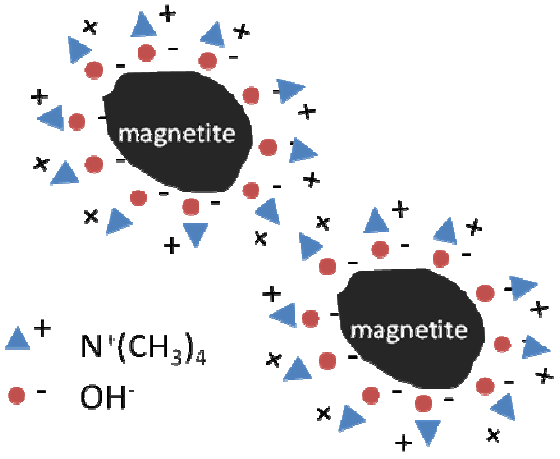

Figure 2.7 Illustration of how magnetite particles are stabilized by surfactant.

2.3.2. Characterization

In this section, various characterization tools employed including high-resolution transmission electron microscopy (HRTEM) (Figure 2.8 (a)), conventional TEM (Figure 2.8 (b) (b)), vibrating sample magnetometer (VSM) (Figure 2.8 (c)) as well as respective results are introduced.

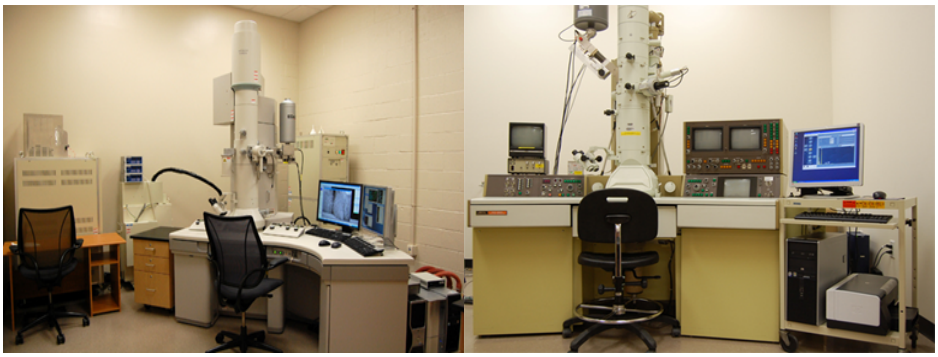

(a) (b)

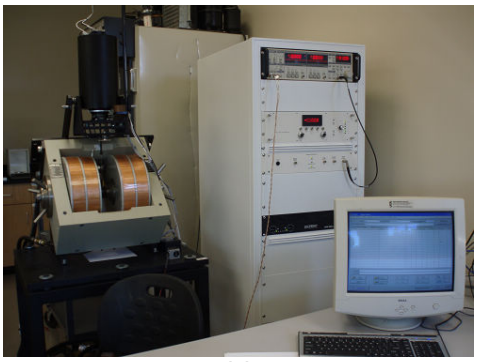

(c)

Figure 2.8: (a) Hitachi H-9500 High-resolution transmission electron microscopy (TEM); (b) JEOL 1200EX transmission electron microscopy (TEM); (c) vibrating sample magnetometer (VSM)

Conventional TEM picture, Figure 2.9, shows that the magnetite particles obtained via co-precipitation method are nearly spherical in shape and exhibit a size distribution from 4 to 16nm. The mean particle size is around 9.6 nm with a standard deviation of 2.53 nm. The size distribution was determined by measuring more than 400 particles form TEM images. It also can

be seen that since no surfactant added, particles somewhat aggregated. Magnetite diffraction pattern indicates that it has a face-centered cubic FCC crystal structure.

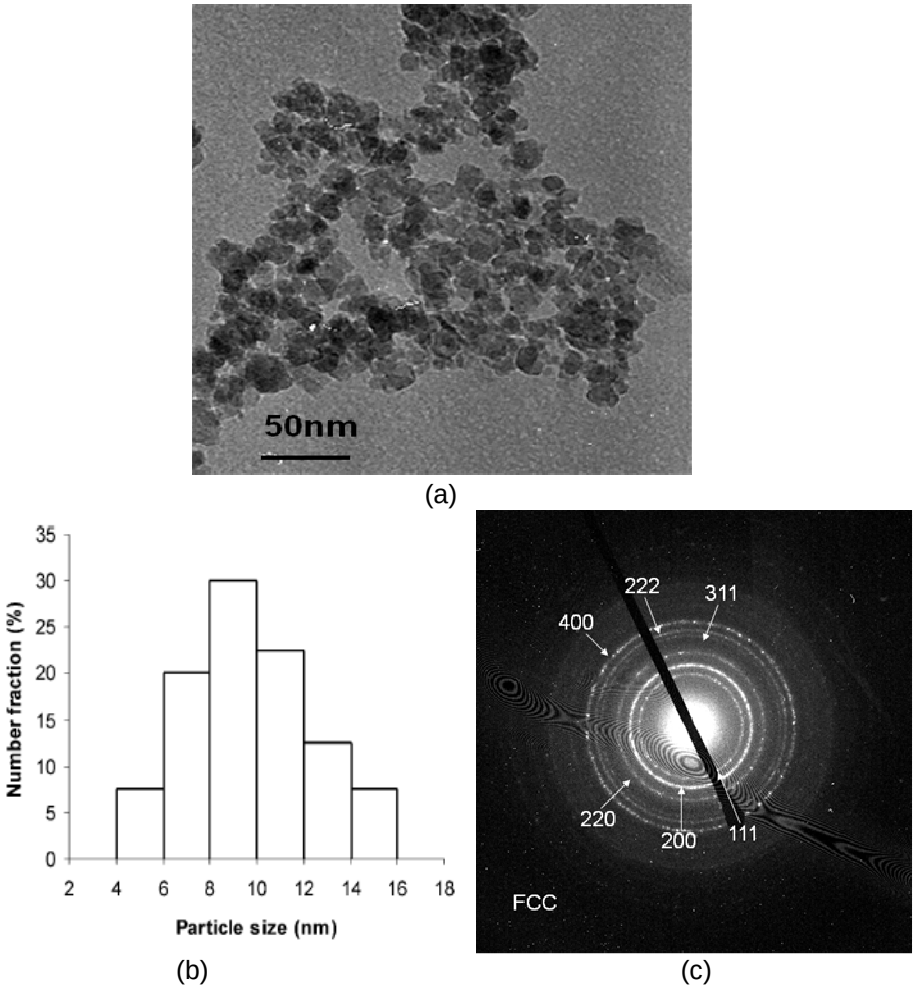

Figure 2.9: (a) TEM image of the magnetite nanoparticles without coating; (b) the size distribution of magnetite nanoparticles; (c) diffraction pattern of magnetite nanocrystal

VSM has been the most popular technique to measure magnetic moment for several decades. This method is based on the magnetic flux change in a coil when a magnetic sample is vibrated near it. In the VSM as shown in Figure 2.10 the sample is mounted to the end of a glass rod; the electromagnet produces a uniform field to magnetize the sample and the field can be swept; the pick-up coils are clamped to the magnet in order to avoid vibration of the coils with respect to the magnet.

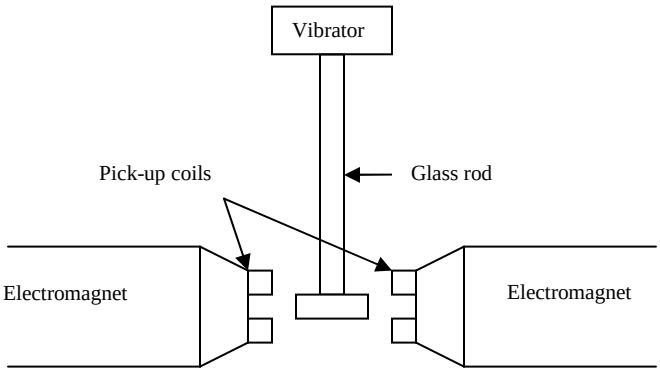

Figure 2.10 Schematic drawing of a vibrating sample magnetometer. The sample is vibrated near a pick-up coil, and the magnetic flux change is detected, which is proportional to the magnetic moment of the sample.

During the measurement, the sample is vibrated at small amplitude with a frequency of ~70Hz, which produces a field distortion in an AC manner. The field distortion is detected by pick-up coil and then is processed with conventional AC processing equipment. The sample's magnetic moment is obtained according to Faraday law of induction, namely that a potential drop, V, is induced across the pick-up coils due to a change of flux:

$$V = -N \, d\Phi/dt$$

Where N is the number of turns in the detection coils and Ø is the flux in the coils, which is proportional to the magnetic moment of the sample.

A VSM usually has a sensitivity of about 10-6 emu.

Magnetic properties of magnetite nanoparticles were measured by VSM. Magnetization loop of non-coated Fe_3O_4 nanoparticles and surfactant-coated magnetite nanoparticles measured at the room temperature are depicted in Figure 2.11.

The results show that no hysteresis is detected. The superparamagnetic behavior is indicated by zero remanence and zero coercivity on the magnetization curves for non-coated magnetite nanoparticles and surfactant-coated magnetite nanoparticles.

Normalized magnetization of magnetite nanoparticles in water and in surfactant (Figure 2.11) shows similar extent to be magnetized under same externally applied field.

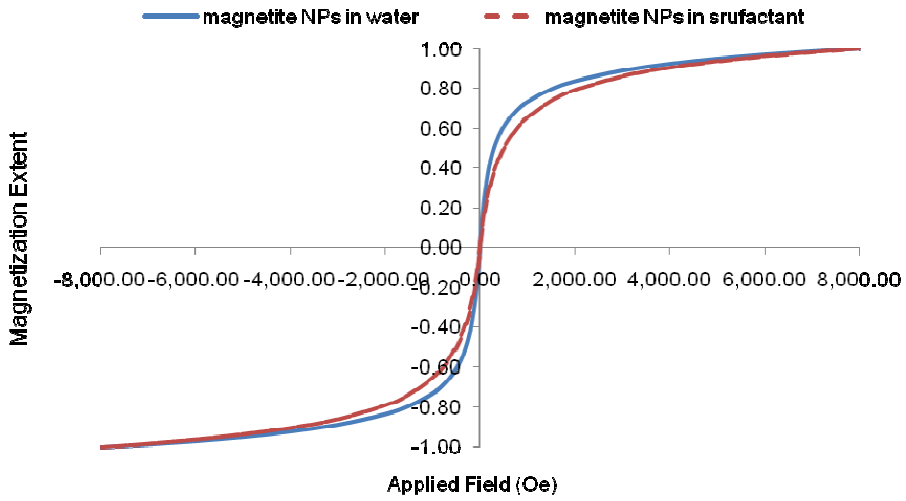

Figure 2.11 Normalized magnetization of non- and surfactant-coated magnetite NPs.

2.3.3. Size Selection

Although co-precipitation is an easy and inexpensive method to prepare magnetite nanoparticles, the experimental challenge in this method lies in control of the particle size and thus achieving a narrow particle size distribution. Since the blocking temperature depends on particle size, a wide particle size distribution will result in a wide range of blocking temperatures and therefore non-ideal magnetic behavior for many applications. Unfortunately, as shown in Figure 2.9 (b), particles prepared by co-precipitation unfortunately tend to be rather polydisperse. Also, as surfactant (tetramethylammonium hydroxide) was added after the co-precipitation process, agglomeration is inevitable in this case.

In order to obtain better dispersed magnetite nanoparticles with smaller size and narrower size distribution, the originally prepared suspension of magnetite nanoparticles in surfactant was centrifuged for 10 min at the speed of 10K rpm, resulting in a stratified suspension where the heavier/bigger or aggregated magnetite nanoparticles are supposed to

settle at the bottom. Figure 2.12 (a) and (b) illustrates the suspension of magnetite nanoparticles before and after centrifugation respectively.

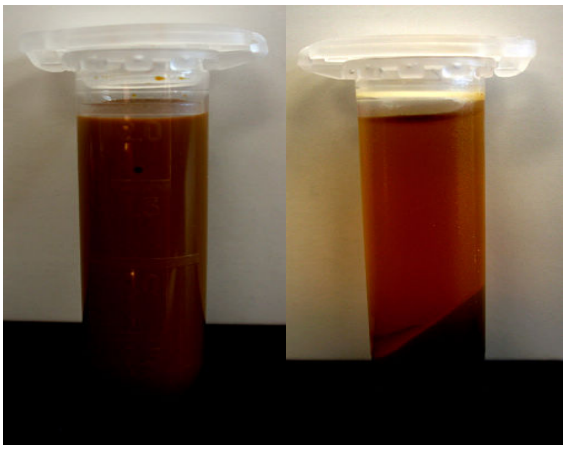

(a) (b)

Figure 2.12(a) original prepared suspension of magnetite nanoparticles in surfactant; (b) stratified suspension of magnetite nanoparticles after centrifugation.

HRTEM image, Figure 2.13 (a), shows that the magnetite nanoparticles in the upper layer of suspension after centrifugation are almost identically spherical in shape and exhibit a size distribution from 4 to 6nm. The mean particle size is around 5 nm with a narrow size distribution. Moreover, from HRTEM image (Figure 2.13 (a)), 2D lattices of an individual nanoparticle can be seen clearly; the lattice fringes 0.48 and 0.25nm observed correspond respectively to interplanar spacings of the (111) and (311) planes for cubic phase magnetite. On the other hand, the magnetite nanoparticles settled down at the bottom have a size distribution from 8nm to 16nm. The mean particle size is nearly 10nm (Figure 2.13 (b)). Furthermore, it can be seen from the image that the lattice distance is about 0.25nm, corresponding to the interplanar space of the (311) planes for cubic phase magnetite.

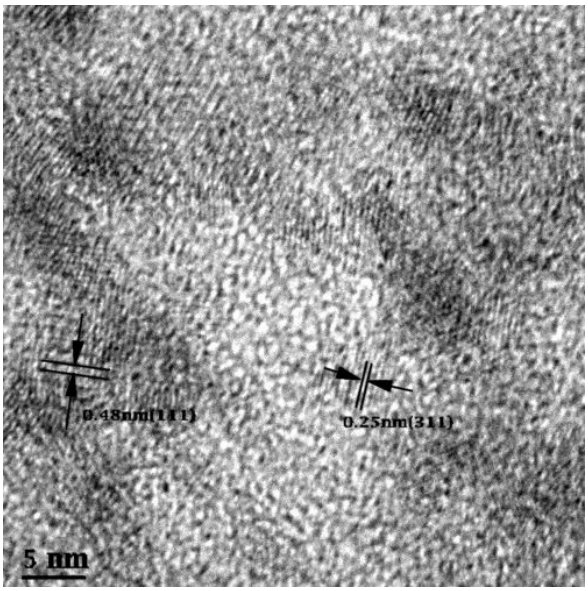

(a)

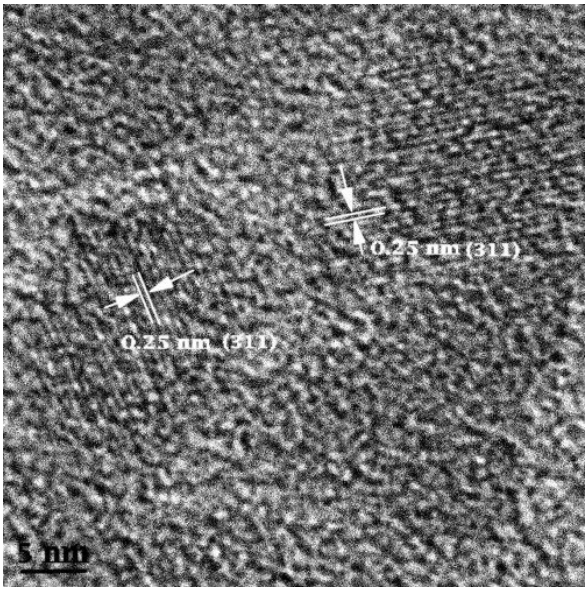

(b)

Figure 2.13 HRTEM pictures of magnetite nanoparticles (a) in the upper layer of suspension and (b) ones settled down at the bottom of the tube after centrifugation.

VSM results of original suspension of magnetite nanoparticles in surfactant, magnetite nanoparticles in upper layer of suspension and those settled down at the bottom after centrifugation are as shown in Figure 2.14 (a), which indicates that the magnetization of

magnetite nanoparticles in the sediment after centrifugation is similar to that of those in the original suspension while the magnetization of magnetite nanoparticles in the upper layer after centrifuging shows much lower magnetization under the same applied field. The extremely low magnetization of magnetite nanoparticles in the upper layer supposed to be due to the small size of nanoparticles of which big amount of magnetization is lost because of the surface phenomenon. It has been mentioned before that the magnetite nanoparticles in the upper layer have very tiny particle size resulting in huge surface areas. It is also known that surfaces including the outer layer and second layer (which occupy nearly 60% volume of the whole particle) of particles are not magnetic. This surface phenomenon makes the magnetization of magnetite nanoparticles in the upper layer extremely low.

The magnetizations are normalized respectively as shown in Figure 2.14 (b) in order to demonstrate and compare the magnetization extent of above mentioned magnetite nanoparticles in different conditions. It is indicated that the smaller magnetite nanoparticles in the upper layer suspension is more difficult to be magnetized comparing with those in the sediment and in original suspension. It is known from the size effect that when the particle size becomes smaller, they tend to be easily randomized by the thermal energy thus more externally applied field is required to bring them to saturation state.

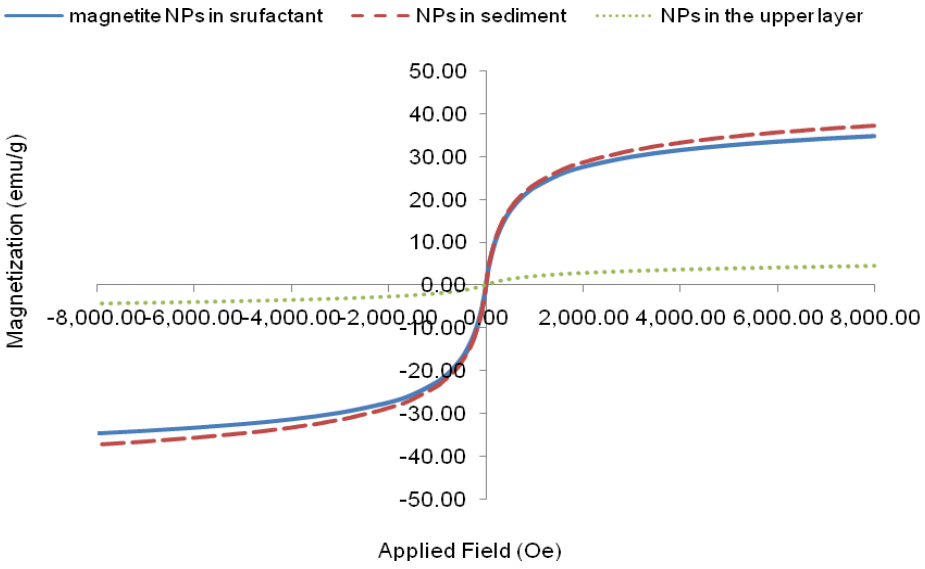

(a)

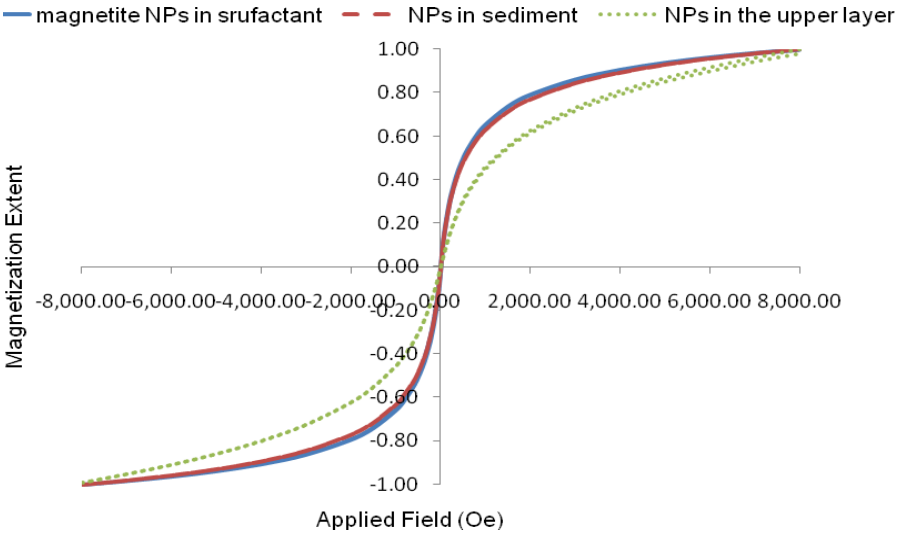

(b)

Figure 2.14 (a) Magnetization of magnetite nanoparticles in original suspension, in upper layer of suspension and in sediment after centrifugation versus applied field. (b) Normalization of magnetizations

2.3.4. Conclusion

Magnetite nanoparticles have been prepared by chemical co-precipitation method and studied for their physical and magnetic properties. Conventional TEM results indicate that the magnetite nanoparticles are nearly spherical in shape and exhibit a wide size distribution from 4 nm to 16 nm. The mean particle size is around 9.6 nm. Suspension of magnetite nanoparticles was obtained by using tetramethylammonium hydroxide as surfactant. VSM results show superparamagnetic behavior of both non-coated and surfactant-coated magnetite nanoparticles and the similar extent to be magnetized under the same applied field. It is also observed that the magnetization decreases in the case of surfactant-coated magnetite nanoparticles due to the less amount of magnetite contained in the same weight of sample.

By centrifuging the original suspension of magnetite nanoparticles in surfactant for 10 min at the speed of 10K rpm, a stratified suspension was obtained where the upper layer contains magnetite nanoparticle with mean size of 5 nm and much narrower size distribution as well as better distribution/less aggregation of nanoparticles while those in the sediment have a mean size of 10nm and more aggregation. Furthermore, it can be seen from VSM results that magnetite nanoparticles in the upper layer have weak magnetization and are more difficult to be magnetized due to the size effect.

CHAPTER 3

DIP-PEN NANOLITHOGRAPHICAL PATTERNING OF MAGNETITE NANOPARTICLES

3.1 Dip-pen Nanolithography

Lithographic methods play an important role in nanotechnology, molecular electronics and modern-time microfabrication. Dip-pen, where ink coated on a sharp tip is transported to paper sheets through capillary forces, was first used nearly 4000 years ago [72] and has been developed to transport molecules on macroscale throughout the history. In 1999, Mirkin's group in Northwestern University invented the so-called "Dip-pen Nanolithography" (DPN) as a new tool to deliver different kinds of molecules via a positive printing mode [73] and fabricate nanostructures on surfaces. DPN is an AFM –based direct-write lithographic technique where the AFM tip is used as a "pen", a solid-state substrate as "paper", and molecules which has good affinity to the substrate as "ink" [73]. In most cases, ink molecules transport from the "pen" to the "paper" through or over a water meniscus which is formed via capillary condensation (Figure 3.1) [74].

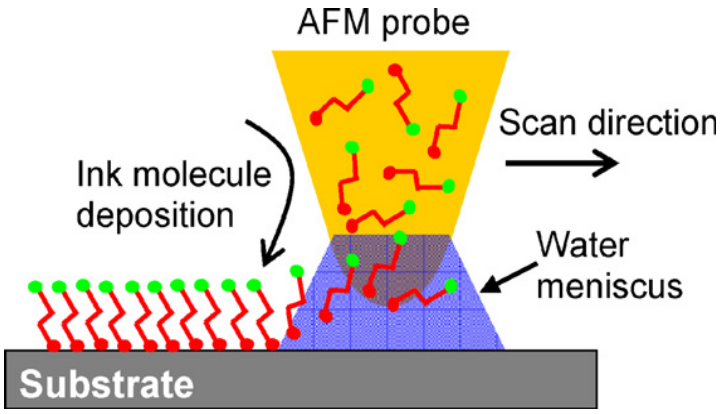

Figure 3.1 Schematic representation of DPN showing the transport of ink from the AFM tip to the substrate through a water meniscus [74].

3.1.1. Ink-substrate Combinations of DPN

Various structures created by DPN depend on the selection of "ink–substrate" combinations. DPN is compatible with many inks ranging from small organic molecules [73, 75-79] to organic [80-82] and biological [83-84] polymers; from colloidal particles [85-87] to metal ions [81, 88-89] and sols [90-92]. DPN related "paper" substrate can be surfaces of insulators, metals and semiconductors. Moreover, DPN can be used to pattern on top of functional monolayers adsorbed on a variety of surfaces. A summary of the various chemicals used and the systems where they have been applied are listed in Table 3.1 [93].

Table 3.1 Overview of the Various DPN Ink-substrate Combinations in Researches [93].

Ink	Substrate	Notes
Alkylthiols (e.g. ODT and MHA)	Au	15 nm resolution with sharp tips on single crystal surfaces, $<$ 50 nm on polycrystalline surfaces
Ferrocenylthiols	Au	redox active nanostructures
Silazanes	SiO_x, GaAs	patterning on oxides
Proteins	Au, SiO_x	both direct write and indirect assembly
Conjugated polymers	SiO_x	polymer deposition verified spectroscopically and electrochemically
DNA	Au, SiO_x	sensitive to humidity and tip-silanization conditions
Fluorescent dyes	SiO_x	luminescent patterns
Sols	SiO_x	solid-state features
Metal salts	Si, Ge	electrochemical and electroless deposition
Colloidal particles	SiO_x	viscous solution patterned from tip
Alkynes	Si	C—Si bond formation
Alkoxysilanes	SiO_x	humidity control important
ROMP materials	SiO_x	combinatorial polymer brush arrays

3.1.2. DPN: a diffusion model

It has been reported that the 'ink' transport from the tip is mediated by a water meniscus that forms between the tip and the substrate under atmospheric conditions. Two key factors associated with the success of DPN are: a spatially narrow deposition of ink molecules and self-assembly of the functionalized ink molecules chemisorbed onto the substrate and to form a stable monolayer on the surface.

The self-assembly of ink molecules deposited using DPN can be modeled as a two dimensional diffusion with a source (AFM tip) (Figure 3.2) [94]. In a proposed mechanism of ink

transportation, the coming molecular flux from the tip creates a concentration gradient around the tip, and ink molecules subsequently diffuse over the region already occupied by other ink molecules (drawn as filled dots) to be finally trapped by the bare surface of the substrate.

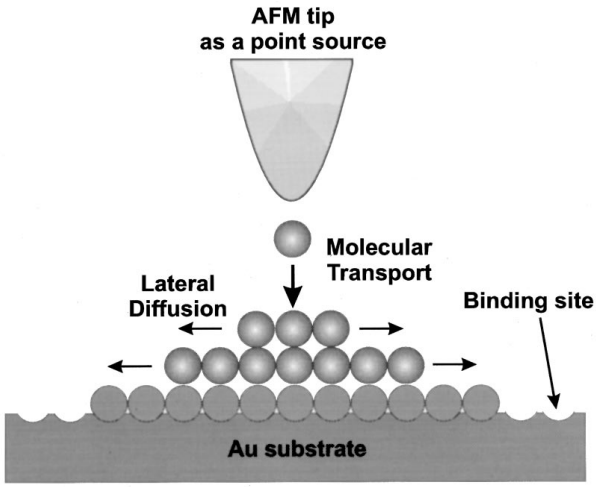

Figure 3.2 Mechanism of ink molecules transporting from the tip to the substrate [94].

If the same amount of ink is deposited, the size of dots generated via fixing the tip position does not depend on the deposition rate. As for a moving tip, however, patterns generated change drastically with the writing speed or the moving rate of the tip.

3.1.3. Comparison of DPN with Other Non-conventional Lithographic Methods

DPN is not the only lithographic tool that allows direct transport of molecules from tips to substrates of interest via a positive printing mode. Other methods, for example, microcontact printing can deposit patterns of thiol-functionalized molecules directly onto Au substrates by using an elastomer stamp [95-96]. This method is a parallel technique, which allows one to deposit an entire pattern or series of patterns on a substrate of interest in one step [97]. One step process is an advantage of microcontact printing over DPN which is a serial technique. However, if one is trying to selectively write various types of molecules at specific positions within a particular type of nanostructure, DPN would outstand. In this regard, DPN complements microcontact printing and many other existing methods of micro- and nanofabrication [97].

Besides positive printing tools, there are several negative printing techniques that rely on scanning probe microscopy (SPM), electron beams (e-beam), or molecular beams to pattern substrates, using self-assembled monolayers (SAMs) and other organic materials as resist layers [98], followed by removing materials for subsequent processing or adsorption steps. However, DPN can deliver relatively small amounts of a molecular substance to a substrate in a nanolithographic fashion that does not rely on a resist, a stamp, complicated processing methods, or sophisticated noncommercial instrumentation [73].

As perhaps the only lithographic technique that offers high resolution as well as registration with capabilities of direct-write printing (Figure 3.3) [93], DPN becomes a particularly attractive method for patterning biological and soft organic structures onto surfaces. These molecules can be deposited in either ambient or inert environments without exposing them to ionizing UV or electron-beam radiation. Additionally, as mentioned before, several different kinds of molecules can be deposited without exposing the substrate to harsh solvents or chemical etchants, thus without risking cross-contamination, the desired chemistry is carried out exactly, and only, where it is needed [99].

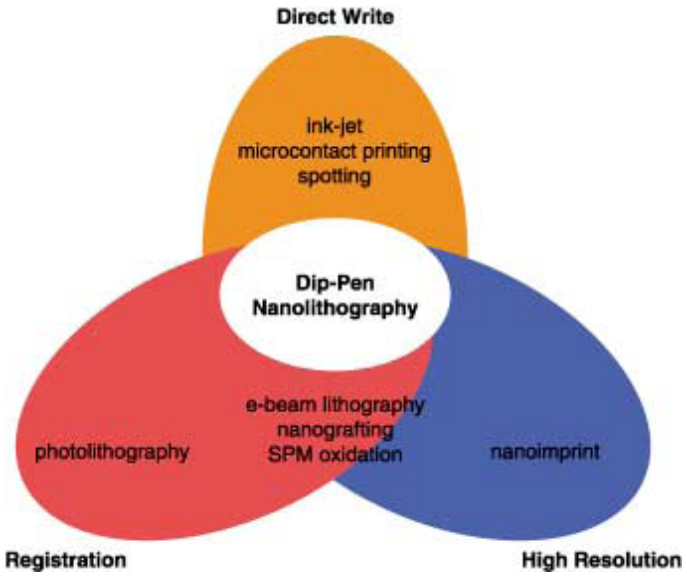

Figure 3.3 Comparison of the capabilities of DPN with various other lithographic tools SPM=scanning probe microscopy [93].

Because of above mentioned advantages and the unique capabilities of DPN, many research groups have started contributing to the development of DPN and using this tool to address important scientific problems inherent to nanostructures. At present, dozens of laboratories around the world have begun to be interested in this technology and to use DPN as a tool in their own research [93]. Research efforts have been made ranging from the fundamentals of tip-substrate ink transport, [100] to the direct deposition of metallic structures and development of electrochemical DPN, [81, 101] to the deposition of biomolecules [102-103] and the effects of DPN on the organization of biopolymers [84].

3.2 Literature Review of DPN Patterning

It has been mentioned in the first chapter that “Dip-pen Nanolithography”, which has been demonstrated as a high-resolution and registration technique to produce patterns from micro- to nanoscale, is compatible to a wide range of “inks”.

Early researches showed that DPN had been used to pattern alkanethiol self-assembled monolayers (SAMs) on Au surface with high resolution and registration [76]. During subsequent years, DPN has been developed to fabricate patterns by organic, inorganic and biological inks. All of these applications will be reviewed respectively in this section.

3.2.1 Fabricating Patterns by Organic Inks

DPN technique has the capability to deliver different sorts of organic materials ranging from thiols and alkynes to silazanes and silanes. These organic inks can be used as materials for direct patterning of nanostructures, as well as templates provided for multiple-step patterning process. In direct patterning, alkylthiols, ODT and MHA for example, have been employed to generate high-resolution structures on both gold and mica surfaces. Silazanes were discovered to be quite suitable to be patterned on semiconductor surfaces which are naturally or thermally oxidized. In the second case, redox-active ferrocenyl-based inks were used to fabricate templates for the orthogonal assembly of nanoparticles [74].

DPN deposition of ODT and MHA on gold/mica substrates has been reported by Piner et al. [73]. ODT SAM was gained by raster scanning an AFM tip which is coated by ODT across the surface. Molecular dot features were obtained by holding the engaged tip at fixed site for certain time periods. Larger ODT dot features were prepared via isotropic diffusion of ODT ink when longer tip-substrate contact time was applied. Besides, ODT arrays and grid were patterned by either holding the tip stationary at one position or scanning line by line. Also, the possible factors that affect the pattern resolution have been discussed by the author. Factors such as roughness of the substrate, ODT ink diffusion, and environmental humidity all contribute to the patterning results.

Subsequently, Hong and co-workers fabricated patterns of multiple organic inks with high registration [76]. As shown in Figure 3.4 (a), a near perfect alignment of MHA dot features generated on an Au (111) surface was demonstrated. A set of MHA dots which are 15nm in diameter was aligned in the shape of capitalized letter “N”. Moreover, they also demonstrated that the patterns generated by an organic ink could be overwritten by another organic ink. Figure 3.1 (b) shows three geometric patterns of MHA. The MHA triangle, square and pentagon were written via scheduled movement of AFM tip coated with MHA ink. After that, the MHA patterns were overwritten with another AFM tip coated with ODT ink by raster scanning several times throughout the substrate surface.

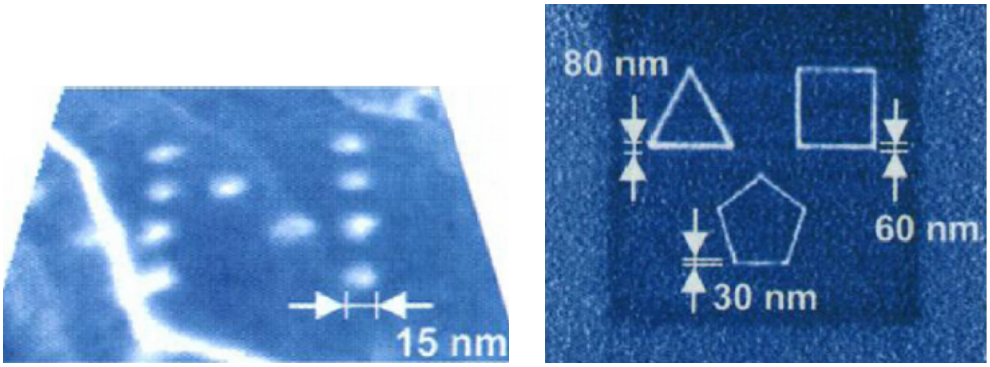

(a) (b)

Figure 3.4 (a) LFM image of a set of MHA dots on Au substrate; (b) MHA patterns overwritten by ODT ink.

Apart from well-studied thiol inks, HMDS has been utilized by Mirkin's group as ink to deliver organic materials onto oxidized silicon and GaAs semiconducting substrate [104]. The reason why they selected HMDS instead of trichlorosilane is because polymerization during ink deposition can be avoided in this way. Stable nanostructures can be fabricated by using HMDS ink due to the irreversible chemisorption of trimethylsilyl (TMS) arising from the reaction of the silazane end group and surface oxides of the substrates. They observed that under nearly identical conditions the writing times required for HMDS on oxidized surfaces are much longer than those for thiol-based inks on Au substrate. However, the writing time need to pattern desired structures can be dramatically reduced by increasing the temperature of the HMDS ink and substrates.

In another research, Ivanisevic et al. reported that redox-active ferrocenylalkylthiol inks could be employed to initiate and guide the assembly of modified nanoparticles in an orthogonal manner [105]. These kinds of inks allowed them to selectively address the ink structures by scanning the potential of an electrode modified with them in linear fashion.

Liu et al. demonstrated the direct writing of monomers on the substrate to form polymer brushes on the nanometer scale [106]. In their work, norbornenylthiol monomers were used as ink to coat the AFM tip which was brought into contact with the Au substrate to define monomer structures. The DPN patterned surface was then used as a template for subsequent molecular passivation, catalyst activation, and ring-opening metathesis polymerization. Dot arrays and line features of the polymer brushes were constructed through the combined DPN and polymerization approach. The feature size, shape, and composition of the polymer brushes could be varied by controlling the choice of the monomer ink, the DPN template, and the polymerization time [74].

3.2.2 Fabricating Patterns by Inorganic Inks

Nanostructures made of inorganic materials such as metals, oxides, and magnetic compounds have been fabricated by Dip-pen Nanolithography. To generate a pattern, the

inorganic inks play two major roles. One is being taken as end materials for single-step deposition; the other is being used as precursors for simultaneous reactions or post-treatments.

Ali et al. reported the direct transfer of Au nanoparticles from the tip to a silica substrate [85]. Thomas et al. claimed that Au and Pd nanocrystals could be directly delivered onto a mica substrate using hydrosols inks [107]. The deposition of Au nanoparticles on SAM-covered Au surface through SAM-Au linkage was demonstrated by Garno et al. [86]. It was reported that Au ionic species could also be used as ink species for DPN writing. In this case, an initial Au (+3) ion was deposited onto the substrate to form elemental Au (0) nanostructures without applying electrochemical conditions through tip biasing [101]. The conversion of soluble Au (+3) ion to insoluble Au (0) metal was due to surface-induced reduction of noble metal ions when they attach to the substrate. Figure 3.5 (a) and (b) schematically shows Au ionic ink transport, and patterns ‘‘DU’’ created using the reductive deposition technique, respectively.

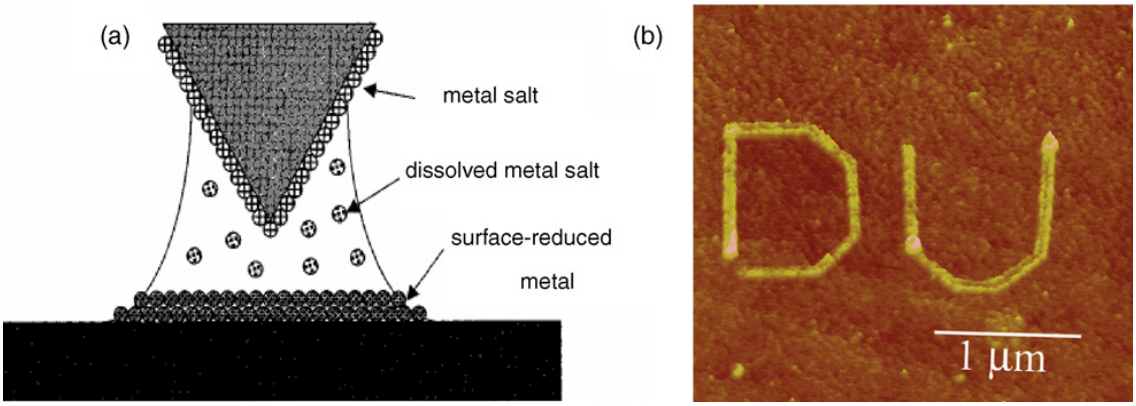

Figure 3.5 (a) Schematic displaying the conversion of Au (+3) ink to Au (0) pattern. (b) LFM image of letter patterns of ‘‘DU’’ written by DPN [101].

Not only single metallic inks, magnetic inorganic compounds can also be transported from the tip to the substrate. γ-Fe_2O_3 nanocrystal inks were applied to fabricate magnetic nanostructures by Gundiah et al. [108]. They reported the creation of magnetic lines with typical widths of 140–200 nm and lengths exceeding 10 mm while no lateral diffusion of ink nanocrystals was observed on silicon and mica substrates.

Fu et al. demonstrated the fabrication of hard magnetic barium hexaferrite (BaFe) nano-patterns through precursor transport and post-heat treatment [90]. In this case, the BaFe precursor was first coated on the tip, and delivered to the substrate to form a precursor pattern. Subsequent thermal annealing of the precursor at elevated temperatures yielded solid-state magnetic structures.

Unlikely, Su and coworkers described a method to fabricate oxide nanostructures via the simultaneous reaction of precursor inks during the DPN process other than post-treatment of the precursor [92]. The oxide patterns were formed by means of the hydrolysis of metal salt precursors in water meniscus through the reaction $2MCl_n + nH_2O \rightarrow M_2O + 2nHCl$. The major substance of the ink is inorganic chlorides MCl_n (where M could be Al, Si, and Sn) which are dissolved in surfactants forming sol–gel-like suspension.

Ding et al. , using a similar approach, patterned the cadmium sulfide (CdS) compound which is a II–VI semiconductor considered having potential applications in the fields of solar cells and light-emitting diodes [109]. The patterning of CdS structures was based on the chemical reaction between Cd^{2+} and S^{2-} precursors during ink transport. Thioacetamide (CH_3CSNH_2, TAA) was used as the sulfide source to react with Cd^{2+} on mica and negatively charged silicon surfaces respectively. Figure 3.6 (a) and (b) shows respectively how precursors react in forming solid-state CdS patterns and CdS features created by using this method. Surface charge, sulfide source and temperature are several parameters that have been found important in generating semiconductor nanostructures. The authors observed and proposed that the static interaction between the negatively charged substrate and the positively charged CdS facilitates the patterning of CdS on the substrate. Considering the selection of sulfide source, if Na_2S or $(NH_4)_2S$ were used, the speed of CdS deposition would be too fast for the inking step of the AFM tip. However, the utilization of TTA, which is compatible with the DPN process, made the violent reaction easier to control. As for temperature, it not only affects the

solubility and diffusion of the precursors, but changes the formation speed of CdS products as well.

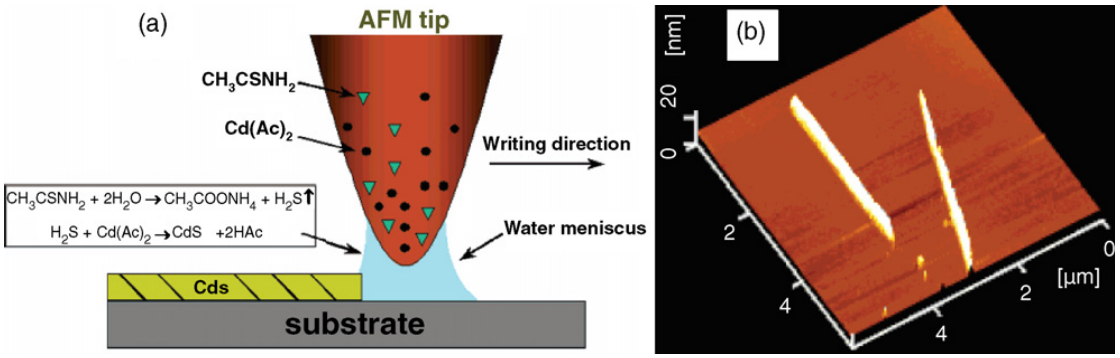

Figure 3.6 (a) Schematic showing the generation of CdS features through the simultaneous reaction of ink precursors. (b) AFM morphology image of CdS patterns created [74].

3.2.3 Fabricating Patterns by Biological Inks

Patterning of biomaterials on nanoscale is of great interest and importance in fabricating biodevices ranging from biosensors and proteomic arrays to gene chips. Several significant factors in creating nanostructures of biological ink via “Dip-pen Nanolithography” have attracted lot of attentions of researchers.

In the first place, proper modification of the AFM probe for the adsorption and desorption of the biological materials is required to carry out effective deposition of biomolecules. Second, the selection of suitable biological inks and substrates is crucial, since the deposition of immobilized biological features depends on the strong interaction between the ink and substrate. Moreover, the important thing is that whether the patterned proteins or DNAs will be able to maintain their original bioactivities.

Taking all the above mentioned factors into consideration, the DPN method should be designed and optimized to meet all requirements. Wilson et al. showed positive printing of collagen and collagen-like peptide with thiolated collagen and peptide inks. Line widths of patterns were down to 30–50 nm [84].

The tip was coated with inks by dipping it into an aqueous ink solution, and then brought to scanning on an Au substrate via DPN. The thiolation modification of the collagen was found to be very crucial to ensure the ink-Au substrate coupling. Immobilization of the patterned collagen ink on Au substrate was due to the sulfhydryl addition. Figure 3.7 [74] (a) shows the AFM phase image of collagen patterns in the shape of letters ‘‘TU’’ on an Au substrate. Biological features patterned via this method could preserve the triple-helical structure and bioactivities of collagen.

Lim et al. directly fabricated antirabbit IgG (immunoglobulin) features on different sort of silicon oxide substrates by applying protein inks [110]. According to their lithographic method, the AFM tip was first modified with a hydrophilic and biocompatible layer in order to prevent protein adsorption and lower the activation energy required for protein transport from the tip to substrates. The substrates used can be either negatively charged or aldehyde-modified oxide surfaces. In this way, protein inks can attach to the surface through electrostatic interaction or covalent bonding. Protein patterns such as line features with line widths down to 55-550 nm have been demonstrated by the authors. Figure 3.7 (b)–(d) are the fluorescence images of different kinds of DPN-generated IgG patterns labeled with a fluorophore. The biorecognition activity of the IgG patterns was also examined, and it was found that antirabbit IgG could selectively bond to rabbit IgG patterns.

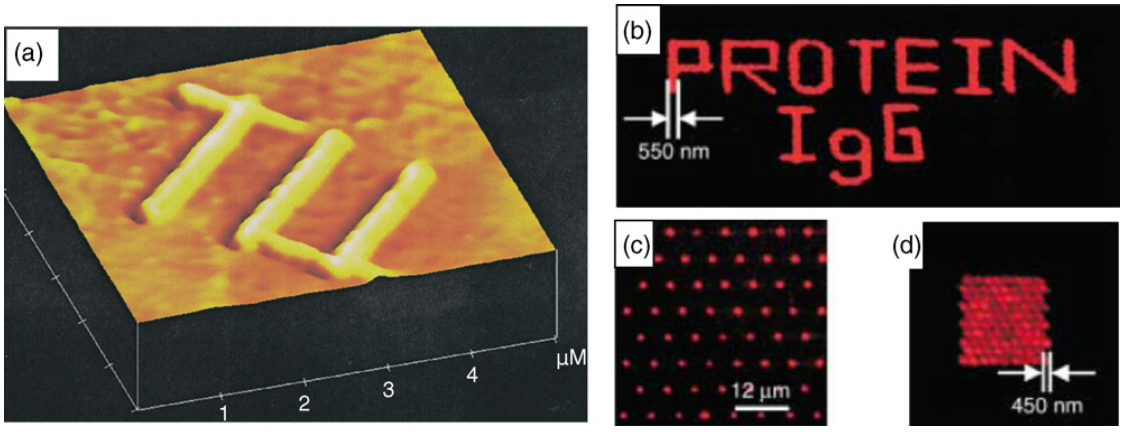

Figure 3.7 (a) AFM phase image of thiolated collagen patterns on Au substrate (b), (c) and (d) show fluorescence images of various antirabbit IgG patterns [74].

Nam et al. showed a relatively simple method for the fabrication of protein nanoarrays with biological activity on nickel oxide surfaces [111]. In their experiments, a Ni layer was coated on the tip to advance the wetting of the tip by His-tagged protein inks via the interaction between the nickel oxide surface and the polyhistidine tag. High humidity conditions were applied to ensure uniformity and rapid protein diffusion, and to inhibit the denaturation of the obtained protein structures on the substrate. N-terminal His-tagged ubiquitin nanoarrays were fabricated in a direct-write fashion in the form of dots and lines. It was observed that protein transport could be made easier on Ni substrate because of the high hydrophilicity of the oxidized surface and its ability to support a water meniscus. The bioactivity of the patterned proteins was confirmed by the observation of the specific binding between labeled anti-ubiquitin molecules and the immobilized ubiquitin nanostructures.

Demers et al., using DNA inks, reported a direct creation of covalently anchored features of oligonucleotides on both metallic and insulating substrates [83]. DNA molecules modified with hexanethiol groups were deposited on Au substrates, while those containing acrylamide could be patterned on silica substrate. Oligonucleotide patterns with feature sizes ranging from micrometers to sub-100 nanometers were generated under different conditions. DNA patterns were found to exhibit sequence-specific binding behavior, and can be used as a template for the direct assembly of individual particles modified with oligonucleotides. Several key factors crucial to DNA patterning were studied, including the surface modification of the tip, and the selection of suitable ink molecules which may have desired affinity to the specific substrates used.

3.3 Experimental

In this section, the overall processes of patterning magnetite nanoparticles via “dip-pen nanolithography” (DPN) as well as DPN under different controlled writing conditions are going to be introduced. Moreover, chemical effects related to DPN will be discussed.

3.3.1 Overall Processes of DPN Patterning of Magnetite Nanoparticles

DPN makes it possible to transport molecules to a substrate, just like a dip-pen transfers ink to paper, however, with the revolution of a conventional atomic force microscope (AFM). 16-Mercaptohexadecanoic acid (MHA), working as ink, was chemisorbed onto the substrate forming a self-assembled monolayer (SAMs) which will subsequently be used as templates for the assembly of different kinds of molecules or nanostructures of interest, for example, magnetic nanoparticles and alkylamine-modified deoxyribonucleic acid (DNA) [112].

In this work, all DPN experiments were carried out with a Dimension 5000 AFM (Figure 3.8 (a)) and commercial available cantilevers (Veeco DNP-10, D triangle, force constant=0.06 N/m, silicon nitride Si_3N_4). Typical ambient conditions of DPN are 45% ± 2% RH humidity and 68℉± 2℉ (NanoFAB Cleanroom). Scanning electron mi croscope (SEM) was employed for pattern characterization (Figure 3.5 (b)).

(a) (b)

Figure 3.8 (a) Veeco Dimension 5000 AFM (Tapping Mode, contact mode, MFM); (b) ZEISS Supra 55 VP SEM

Figure 3.9 shows the working principle of AFM. An AFM tip is mounted on the cantilever. A laser beam shines down on the tip and reflects. As the tip goes up and down the reflected laser hits different parts of the detector which is called position-sensitive detector. Since the information collected is corresponding to different positions, an image of the sample surface can be recreated.

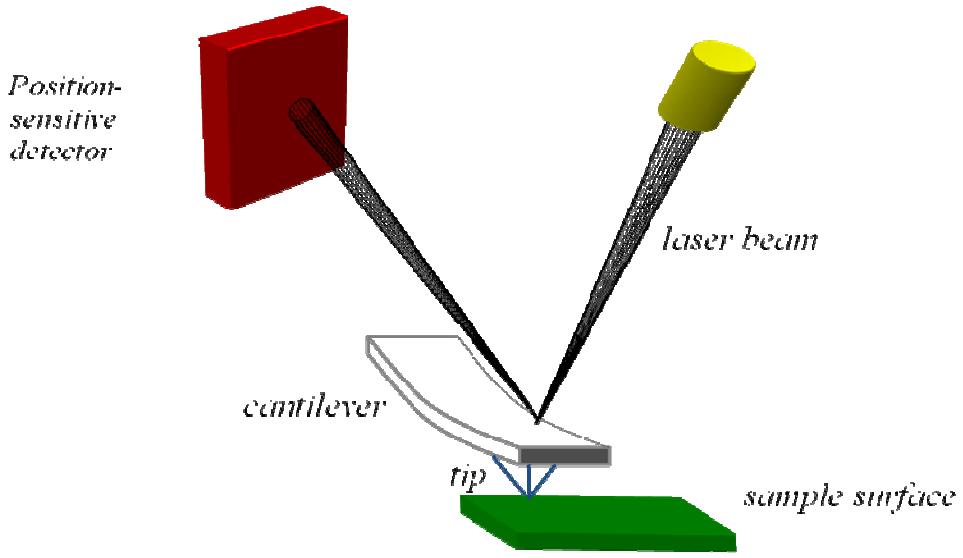

Figure 3.9 Schematic Representation of AFM Working Principle

All chemicals used in DPN experiments including 1-Octadecanethiol (ODT), 16-Mercaptohexadecanoic acid (MHA) and acetonitrile were purchased from Sigma Aldrich and used without further purification.

In a typical patterning process of magnetite nanoparticles, the whole cantilever with a silicon nitride tip already mounted on it was dipped into a saturated solution of MHA in acetonitrile for 15 min in order to coat the tip well with MHA ink. Before being used, the cantilever was blown dry with compressed air.

Under contact mode AFM, the MHA patterns were created by bringing the tip in contact with the gold-coated silicon wafer which was used as substrate and traversing the tip over the gold surface in the form of the desired patterns. MHA, a kind of molecule that has 2 functional groups, carboxyl and thiol groups, can easily anchor onto the gold surface due to the good affinity of thiol group to gold (Figure 3.10 (a)).

In order to form a passivating layer on gold surface around the MHA patterns, the patterned substrate is then dipped into a saturated solution of ODT in acetonitrile for 1 min. ODT is a kind of molecule having only one functional group which is thiol group. Due to the

thiol-gold chemisorption, ODT can be used to passivate the blank areas other than those covered by MHA (Figure 3.10 (b)).

After being rinsed with acetonitrile and blown dry with compressed air, the substrate was treated by dipping into a self-prepared suspension of the magnetite nanoparticles for 30 sec and the dried gently with compressed air. Finally, the specific binding between MHA molecules and magnetite nanoparticles was observed (Figure 3.10 (c)). It was also observed that, at exceeding concentration, non-specific binding between magnetite nanoparticles and ODT molecules existed as well.

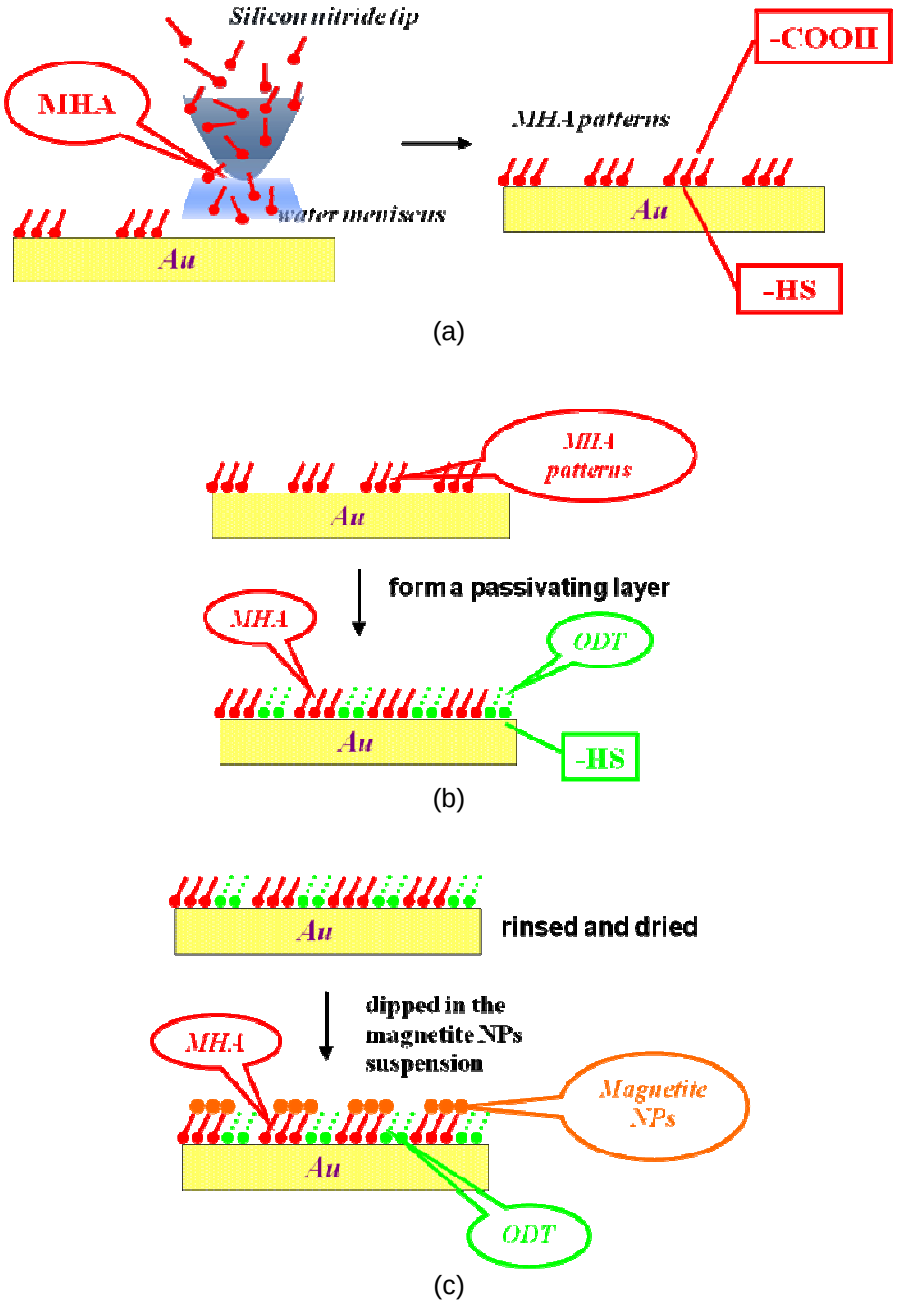

Figure 3.10 schematic representation of the procedures employed to pattern magnetite nanoparticles on gold substrate by DPN

To make it more convenient to find the patterned areas, the substrate is formed via photolithography and lift-off process. Prepared substrate is as in Figure 3.11. Each labeled square is covered by gold, having a size of 100μm^2.

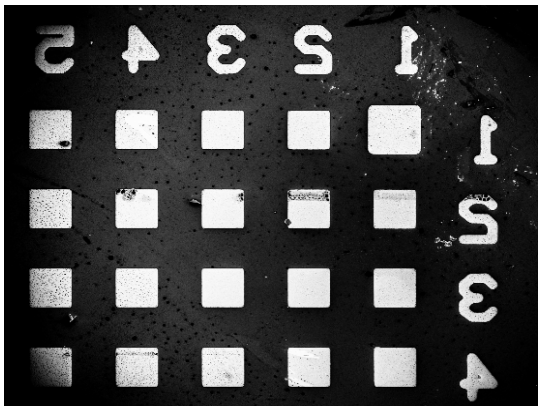

Figure 3.11 the Substrate used for DPN.

3.3.2 DPN Writing Conditions

By using above mentioned strategy, magnetite patterns including dot and line features could be routinely generated, as seen in Figure 3.12 (a) and Figure 3.13 (a) respectively.

As for generating dot-features, the cantilever with silicon nitride tip mounted on it was dipped into a saturated solution of MHA in acetonitrile for 15 min before DPN, so that the tip could be well coated with MHA molecules. After being blown dry with compressed air, the tip was then brought to be in contact with the Au-substrate by using contact mode AFM. The scan size was set to be 0.00μm and the scan speed to be 1Hz. The writing/tip-substrate contact time varied from 3 sec to 40 sec, resulting in the change of dot diameters from 200nm to 700nm respectively. After DPN, the MHA patterned substrate was placed in a saturated solution of ODT in acetonitrile for 1 min to passivate the blank areas around the MHA dot patterns. The substrate was taken out, rinsed with acetonitrile and blown dry with compressed air. Finally, the patterned substrate was dipped into a prepared magnetite nanoparticle suspension for 30 sec and blew dry with condensed air. Generated dot patterns are seen as in Figure 3.12 (a). Figure

3.12 (b), where MHA dot diameter is plotted as a function of writing time t, shows that the dot diameter has the $t^{1/2}$ dependence [77, 104].

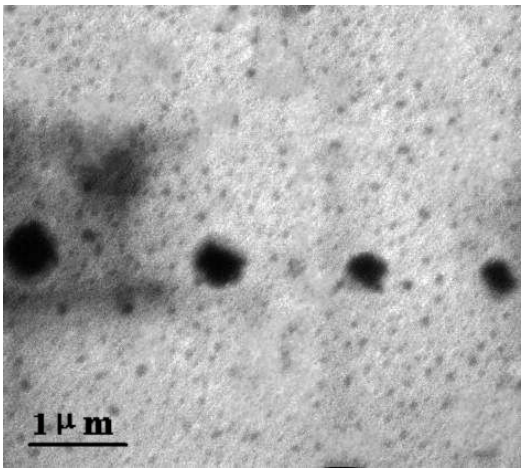

(a)

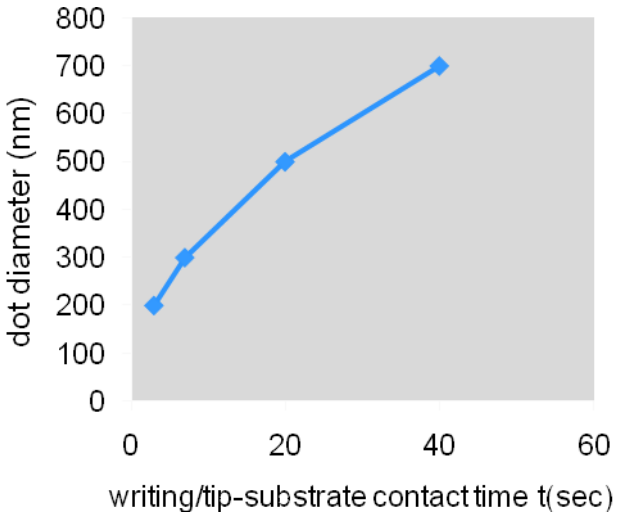

(b)

Figure 3.12 magnetite patterns prepared according to Figure 3.10. (a) (Scanning electron microscope) SEM image of magnetite structures formed on MHA dots generated by increasing the writing/tip-substrate contact time. Time of MHA deposition and measured diameter of the dots are as follows (from right to left): 3 sec, 200nm; 7sec, 300nm; 20sec, 500nm; 40sec, 700nm (b) MHA dot diameter plotted as a function of the writing/tip-substrate contact time.

As for generating line-features, the cantilever with silicon nitride tip mounted on it was dipped into a saturated solution of MHA in acetonitrile for 15 min before DPN to make the tip well coated with MHA molecules. After being blown dry with compressed air, The AFM tip was

engaged by using contact mode AFM and started scanning. The scan size was set to be 80µm×5µm and the writing/scanning time to be 2 min for each line. It was observed that increasing the scanning speed resulted in narrower lines. After DPN, the MHA patterned substrate was dipped into and saturated solution of ODT in acetonitrile for 1 min to passivate the blank areas around the MHA line patterns. The substrate was then taken out, rinsed with acetonitrile and blown dry with compressed air. During the last step, the patterned substrate was placed in a prepared magnetite nanoparticle suspension for 30 sec and blown dry with condensed air. The line-features of magnetite nanoparticles are as seen in Figure 3.13 (a). In Figure 3.13 (b), MHA line width is plotted as a function of writing/scanning speed v, showing that the line width has a linear relationship with the MHA deposition speed [112].

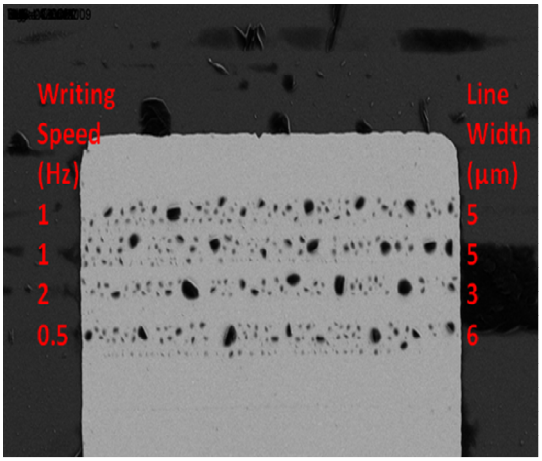

(a)

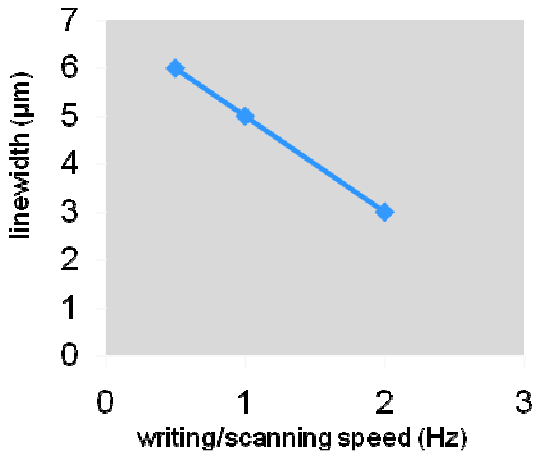

(b)

Figure 3.13 (a) (Scanning electron microscope) SEM image of lines of magnetite structures formed on lines of MHA generated by tuning the scan speed. The speed of MHA deposition and measured width of line features are the following (from top to bottom): 1Hz, 5µm; 1Hz, 5µm; 2Hz, 3µm; 0.5Hz, 6µm. (b) MHA line width plotted as a function of tip writing/scanning speed.

3.3.3 Chemical Interaction/Effects

It has been described in 3.3.1 that chemisorptions of MHA and ODT molecules onto the substrate were due to the good affinity between thiol functional group and gold. Also, surfactant coating outside the magnetite nanoparticles increases their affinity for negatively charged MHA which is attached to gold surface leaving carboxyl functional group pointing out. By doing so, ODT is supposed to passivate areas that are not covered by MHA molecules thus no attachment of magnetite nanoparticles on it.

Unfortunately, non-specific binding was observed as well when the concentration of magnetite nanoparticles exceeded certain value. In other words, magnetite nanoparticles go onto not only MHA but ODT molecules as well. if the concentration of magnetite nanoparticles suspension is too high, ODT will lose the passivation effect. Concentration of magnetite nanoparticles suspension becomes crucial in this case, and it is necessary to determine the specific value of suitable concentration with which there will be good coverage of magnetite nanoparticles on MHA patterns while little or none on ODT passivated areas.

In order to test the attachment effects of magnetite nanoparticles on MHA molecules, a cleaned (Put the Au-coated wafer into a 5:1:1 (v/ v/ v) mixture of H_2O, H_2O_2 and NH_3 at 80℃ for 20mins.) gold coated silicon wafer was dipped into a saturated solution of MHA in acetonitrile for 5 min and blown dry with condensed air. After that, the MHA covered Au substrate was then immersed into a suspension of magnetite nanoparticles in surfactant for 30 sec. SEM pictures show that after diluting the original suspension of magnetite nanoparticles in surfactant for 8 times, the coverage of magnetite nanoparticles on MHA SAMs did not change much (Figure 3.14).

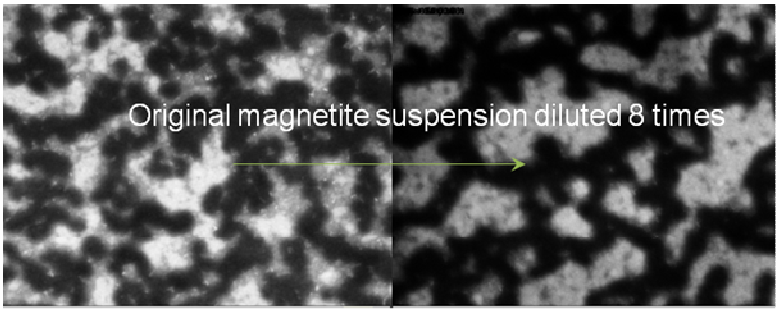

Figure 3.14 Effects of the concentration of magnetite nanoparticles suspension on 16-Mercaptohexadecanoic acid) MHA molecules

For testing the attachment effects of magnetite nanoparticles on ODT molecules, similarly, a cleaned (Put the Au-coated wafer into a 5:1:1 (v/ v/ v) mixture of H_2O, H^2O_2 and NH3 at 80℃ for 20mins.) gold coated silicon wafer was dipped into a saturated solution of ODT in acetonitrile for 1 min and blown dry with condensed air. After that, the ODT passivated Au substrate was then immersed into a suspension of magnetite nanoparticles in surfactant for 30 sec. SEM pictures demonstrate that non-specific binding between ODT molecules and magnetite nanoparticles was observed by dipping the substrate into the original suspension of magnetite nanoparticles in surfactant. After diluting the original suspension 8 times, ODT was able to be used to passivate the gold surface (Figure 3.15).

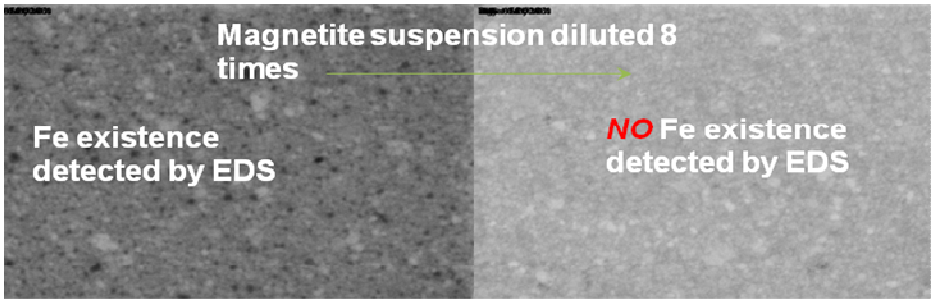

Figure 3.15 Effects of the concentration of magnetite nanoparticles suspension on 1-Octadecanethiol (ODT) molecules

Finally, the optimum concentration was determined by diluting the original suspension of magnetite nanoparticles in surfactant for 8 times before being used in DPN experiments. Effects of optimum concentration of magnetite nanoparticles suspension on MHA and ODT coated

substrates are shown in Figure 3.16. It can be clearly seen that magnetite nanoparticles could differentiate one kind of molecules from another and the preference is obvious under this concentration of magnetite nanoparticles suspension.

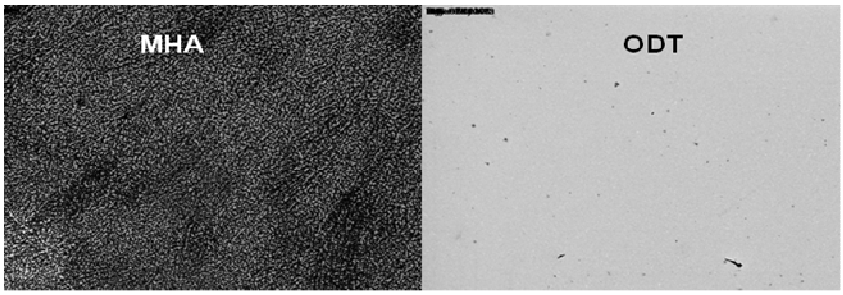

Figure 3.16 Compare effects of magnetite nanoparticles attachment on MHA and ODT using the same concentration of magnetite suspension (original suspension diluted for 8 times)

The exact concentration was calculated after drying (the boiling point of the surfactant: 60-65℃; set the heating temperature to 150℃) and weighing 1 ml original magnetite nanoparticles in suspension diluted for 8 times. M (NPs) (used in the DPN experiments) equals to 0.00545mol/L and the number of NPs per Liter solvent is 3.281×10^{21}.

3.4 Conclusion

An overall process for DPN patterning of magnetite nanoparticles has been introduced. In a typical DPN experiment, the whole cantilever with a silicon nitride tip mounted on it was dipped into a saturated solution of MHA in acetonitrile for 15 min in order to coat the tip well with MHA ink. Blow-dry the tip with compressed air before being used. By using contact mode AFM, the MHA patterns were created by bringing the tip in contact with the gold-coated silicon wafer traversing the tip over the gold surface in the form of the desired patterns, dots or lines for example. The MHA patterned substrate is then dipped into a saturated solution of ODT in acetonitrile for 1 min to passivate the blank areas that are not covered by MHA molecules on gold surface. Take it out and blow-dry with condensed air before dipping into a suspension of magnetite nanoparticles in surfactant which has a specified concentration.

As expected, the size of the magnetite dots and lines generated in these experiments correlates with the size of the MHA dot and line templates created by DPN. More importantly, the diameter of MHA dot features could be controlled by adjusting the tip-substrate contact time, which exhibits the $t^{1/2}$ dependence [2, 3] , Figure 3.12 (b); the width of MHA line features could be controlled by tuning the scan speed, which is supposed to have a linear relationship with the line width, Figure 3.13 (b). These experiments indicate that structures with precise control over feature size and shape could be generated routinely via DPN.

It has been also demonstrated that the concentration of suspension of magnetite nanoparticles is crucial to the passivating effect of ODT. The optimum value of concentration of the suspension was investigated to be 0.00545mol/L, under which good coverage of magnetite nanoparticles on MHA patterns and less/none binding between ODT molecules and magnetite nanoparticles were observed.

REFERENCES

1. Mathew, D.S. and R.S. Juang, *An overview of the structure and magnetism of spinel ferrite nanoparticles and their synthesis in microemulsions.* Chemical Engineering Journal, 2007. **129**(1-3): p. 51-65.
2. Vestal, C.R. and Z.J. Zhang, *Magnetic spinel ferrite nanoparticles from microemulsions.* International Journal of Nanotechnology, 2004. **1**(1-2): p. 240-263.
3. L.Neel, *PROPRIETES MAGNETIQUES DES FERRITES - FERRIMAGNETISME ET ANTIFERROMAGNETISME.* ANNALES DE PHYSIQUE 1948. **3**.
4. Sugimoto, M., *The past, present, and future of ferrites.* Journal of the American Ceramic Society, 1999. **82**(2): p. 269-280.
5. *http://www.msm.cam.ac.uk/doitpoms/tlplib/ferromagnetic/printall.php*.
6. Lu, A.H., E.L. Salabas, and F. Schuth, *Magnetic nanoparticles: Synthesis, protection, functionalization, and application.* Angewandte Chemie-International Edition, 2007. **46**(8): p. 1222-1244.
7. Teja, A.S. and P.Y. Koh, *Synthesis, properties, and applications of magnetic iron oxide nanoparticles.* Progress in Crystal Growth and Characterization of Materials, 2009. **55**(1-2): p. 22-45.
8. Batlle, X. and A. Labarta, *Finite-size effects in fine particles: magnetic and transport properties.* Journal of Physics D-Applied Physics, 2002. **35**(6): p. R15-R42.
9. A.H.Morrish, ed. *The Physical Principles of Magnetism*. 1965, Wiley: New York.
10. Tartaj, P., *Superparamagnetic Composites: Magnetism with No Memory.* European Journal of Inorganic Chemistry, 2009(3): p. 333-343.
11. *http://www.tu-chemnitz.de/physik/OFGF/research/magnetic_recording.php*.

12. C.M.SORENSEN, ed. *Magneticsm in Nanoscale Materials in Chemistry*. 2001, Wiley-interscience Publication: New York.

13. Grasset, F., et al., *Synthesis and magnetic characterization of zinc ferrite nanoparticles with different environments: Powder, colloidal solution, and zinc ferrite-silica core-shell nanoparticles.* Langmuir, 2002. **18**(21): p. 8209-8216.

14. Neveu, S., et al., *Size-selective chemical synthesis of tartrate stabilized cobalt ferrite ionic magnetic fluid.* Journal of Colloid and Interface Science, 2002. **255**(2): p. 293-298.

15. Sun, S.H. and H. Zeng, *Size-controlled synthesis of magnetite nanoparticies.* Journal of the American Chemical Society, 2002. **124**(28): p. 8204-8205.

16. Chen, Q., et al. *Synthesis of superparamagnetic MgFe2O4 nanoparticles by coprecipitation*: Elsevier Science Bv.

17. Park, J., et al., *Ultra-large-scale syntheses of monodisperse nanocrystals.* Nature Materials, 2004. **3**(12): p. 891-895.

18. Majewski, P. and B. Thierry, *Functionalized magnetite nanoparticles - Synthesis, properties, and bio-applications.* Critical Reviews in Solid State and Materials Sciences, 2007. **32**(3-4): p. 203-215.

19. Chastellain, A., A. Petri, and H. Hofmann, *Particle size investigations of a multistep synthesis of PVA coated superparamagnetic nanoparticles.* Journal of Colloid and Interface Science, 2004. **278**(2): p. 353-360.

20. Jolivet, J.P. and E. Tronc, *INTERFACIAL ELECTRON-TRANSFER IN COLLOIDAL SPINEL IRON-OXIDE - CONVERSION OF FE3O4-GAMMA-FE2O3 IN AQUEOUS-MEDIUM.* Journal of Colloid and Interface Science, 1988. **125**(2): p. 688-701.

21. Khaleel, A.A., *Nanostructured pure gamma-Fe2O3 via forced precipitation in an organic solvent.* Chemistry-a European Journal, 2004. **10**(4): p. 925-932.

22. Kim, D.K., et al. *Synthesis and characterization of surfactant-coated superparamagnetic monodispersed iron oxide nanoparticles*: Elsevier Science Bv.

23. Liu, Z.L., et al., *Synthesis and characterization of ultrafine well-dispersed magnetic nanoparticles.* Journal of Magnetism and Magnetic Materials, 2004. **283**(2-3): p. 258-262.

24. Tronc, E., et al., *TRANSFORMATION OF FERRIC HYDROXIDE INTO SPINEL BY FE(II) ADSORPTION.* Langmuir, 1992. **8**(1): p. 313-319.

25. Y.Tamaura, Journal of the Chemical Society Dalton Transactions, 1983(2): p. 189-194.

26. Kim, D.K., et al., *Protective coating of superparamagnetic iron oxide nanoparticles.* Chemistry of Materials, 2003. **15**(8): p. 1617-1627.

27. Lin, C.L., C.F. Lee, and W.Y. Chiu, *Preparation and properties of poly(acrylic acid) oligomer stabilized superparamagnetic ferrofluid.* Journal of Colloid and Interface Science, 2005. **291**(2): p. 411-420.

28. Lee, J.W., T. Isobe, and M. Senna, *Magnetic properties of ultrafine magnetite particles and their slurries prepared via in-situ precipitation.* Colloids and Surfaces a-Physicochemical and Engineering Aspects, 1996. **109**: p. 121-127.

29. Khalafalla, S.E. and G.W. Reimers, *PREPARATION OF DILUTION-STABLE AQUEOUS MAGNETIC FLUIDS.* Ieee Transactions on Magnetics, 1980. **16**(2): p. 178-183.

30. Wooding, A., M. Kilner, and D.B. Lambrick, *STUDIES OF THE DOUBLE SURFACTANT LAYER STABILIZATION OF WATER-BASED MAGNETIC FLUIDS.* Journal of Colloid and Interface Science, 1991. **144**(1): p. 236-242.

31. Redl, F.X., et al., *Magnetic, electronic, and structural characterization of nonstoichiometric iron oxides at the nanoscale.* Journal of the American Chemical Society, 2004. **126**(44): p. 14583-14599.

32. Sun, S.H., et al., *Monodisperse MFe2O4 (M = Fe, Co, Mn) nanoparticles.* Journal of the American Chemical Society, 2004. **126**(1): p. 273-279.

33. Kwon, S.G., et al., *Kinetics of monodisperse iron oxide nanocrystal formation by "heating-up" process.* Journal of the American Chemical Society, 2007. **129**(41): p. 12571-12584.

34. Bronstein, L.M., et al., *Influence of iron oleate complex structure on iron oxide nanoparticle formation.* Chemistry of Materials, 2007. **19**(15): p. 3624-3632.

35. Jung, H., et al., *Preparation of riotic and abiotic iron oxide nanoparticles (IOnPs) and their properties and applications in heterogeneous catalytic oxidation.* Environmental Science & Technology, 2007. **41**(13): p. 4741-4747.

36. Li, Z., et al., *One-pot reaction to synthesize biocompatible magnetite nanoparticles.* Advanced Materials, 2005. **17**(8): p. 1001-+.

37. Pinna, N., et al., *Magnetite nanocrystals: Nonaqueous synthesis, characterization, and solubility.* Chemistry of Materials, 2005. **17**(11): p. 3044-3049.

38. Capek, I., *Preparation of metal nanoparticles in water-in-oil (w/o) microemulsions.* Advances in Colloid and Interface Science, 2004. **110**(1-2): p. 49-74.

39. Pang, Y.X. and X.J. Bao, *Aluminium oxide nanoparticles prepared by water-in-oil microemulsions.* Journal of Materials Chemistry, 2002. **12**(12): p. 3699-3704.

40. Pillai, V., et al., *PREPARATION OF NANOPARTICLES OF SILVER-HALIDES, SUPERCONDUCTORS AND MAGNETIC-MATERIALS USING WATER-IN-OIL MICROEMULSIONS AS NANO-REACTORS.* Advances in Colloid and Interface Science, 1995. **55**: p. 241-269.

41. Tartaj, P. and L.C. De Jonghe, *Preparation of nanospherical amorphous zircon powders by a microemulsion-mediated process.* Journal of Materials Chemistry, 2000. **10**(12): p. 2786-2790.

42. Tavakoli, A., M. Sohrabi, and A. Kargari, *A review of methods for synthesis of nanostructured metals with emphasis on iron compounds.* Chemical Papers, 2007. **61**(3): p. 151-170.

43. Eckert, C.A., B.L. Knutson, and P.G. Debenedetti, *Supercritical fluids as solvents for chemical and materials processing.* Nature, 1996. **383**(6598): p. 313-318.

44. Hao, Y.L. and A.S. Teja, *Continuous hydrothermal crystallization of alpha-Fe2O3 and Co3O4 nanoparticles.* Journal of Materials Research, 2003. **18**(2): p. 415-422.

45. Cabanas, A., et al., *Continuous hydrothermal synthesis of inorganic materials in a near-critical water flow reactor; the one-step synthesis of nano-particulate Ce1-xZrxO2 (x=0-1) solid solutions.* Journal of Materials Chemistry, 2001. **11**(2): p. 561-568.

46. Lam, U.T., et al., *Processing of iron oxide nanoparticles by supercritical fluids.* Industrial & Engineering Chemistry Research, 2008. **47**(3): p. 599-614.

47. Sue, K., et al., *Size-controlled synthesis of metal oxide nanoparticles with a flow-through supercritical water method.* Green Chemistry, 2006. **8**(7): p. 634-638.

48. Wang, X., et al., *A general strategy for nanocrystal synthesis.* Nature, 2005. **437**(7055): p. 121-124.

49. Deng, H., et al., *Monodisperse magnetic single-crystal ferrite microspheres.* Angewandte Chemie-International Edition, 2005. **44**(18): p. 2782-2785.

50. Burda, C., et al., *Chemistry and properties of nanocrystals of different shapes.* Chemical Reviews, 2005. **105**(4): p. 1025-1102.

51. Shaw, R.W., et al., *SUPERCRITICAL WATER - A MEDIUM FOR CHEMISTRY.* Chemical & Engineering News, 1991. **69**(51): p. 26-39.

52. Sue, K., K. Kimura, and K. Arai, *Hydrothermal synthesis of ZnO nanocrystals using microreactor.* Materials Letters, 2004. **58**(25): p. 3229-3231.

53. Hermanek, M., et al., *Catalytic efficiency of iron(III) oxides in decomposition of hydrogen peroxide: Competition between the surface area and crystallinity of nanoparticles.* Journal of the American Chemical Society, 2007. **129**(35): p. 10929-10936.

54. Xu, Z.P., et al., *Inorganic nanoparticles as carriers for efficient cellular delivery.* Chemical Engineering Science, 2006. **61**(3): p. 1027-1040.

55. Bergemann, C., et al. *Magnetic ion-exchange nano- and microparticles for medical, biochemical and molecular biological applications*: Elsevier Science Bv.

56. Giri, S., et al., *Stimuli-responsive controlled-release delivery system based on mesoporous silica nanorods capped with magnetic nanoparticles.* Angewandte Chemie-International Edition, 2005. **44**(32): p. 5038-5044.

57. Nunez, L. and M.D. Kaminski. *Transuranic separation using organophosphorus extractants adsorbed onto superparamagnetic carriers*: Elsevier Science Bv.

58. R.M.CORNELL, ed. *The Iron Oxides: Structure, Properties, Reactions, Occurrences and Uses*. second ed. 2003, Wiley-VCH.

59. Tartaj, P., et al., *The preparation of magnetic nanoparticles for applications in biomedicine.* Journal of Physics D-Applied Physics, 2003. **36**(13): p. R182-R197.

60. Kim, J.S., et al., *Toxicity and tissue distribution of magnetic nanoparticles in mice.* Toxicological Sciences, 2006. **89**(1): p. 338-347.

61. Tartaj, P., et al. *Advances in magnetic nanoparticles for biotechnology applications*: Elsevier Science Bv.

62. Yang, H.H., et al., *Magnetite-containing spherical silica nanoparticles for biocatalysis and bioseparations.* Analytical Chemistry, 2004. **76**(5): p. 1316-1321.

63. Wang, S.X., et al. *Towards a magnetic microarray for sensitive diagnostics*: Elsevier Science Bv.

64. Lubbe, A.S., et al., *Clinical experiences with magnetic drag targeting: A phase I study with 4'-epidoxorubicin in 14 patients with advanced solid tumors.* Cancer Research, 1996. **56**(20): p. 4686-4693.

65. Neuberger, T., et al. *Superparamagnetic nanoparticles for biomedical applications: Possibilities and limitations of a new drug delivery system*: Elsevier Science Bv.

66. Kohler, N., et al., *Methotrexate-modified superparamagnetic nanoparticles and their intracellular uptake into human cancer cells.* Langmuir, 2005. **21**(19): p. 8858-8864.

67. Reimers, G.W., *Preparing magnetic fluids by a peptizing method.* 1972. **59**.

68. Fu, L., V.P. Dravid, and D.L. Johnson, *Self-assembled (SA) bilayer molecular coating on magnetic nanoparticles.* Applied Surface Science, 2001. **181**(1-2): p. 173-178.

69. F.A.Cotton, ed. *Advanced inorganic chemistry*. 1988, Wiley Interscience: New York.

70. R.M.CORNELL, ed. *Iron oxides in the laboratory; preparation and characterization* 1991, Weinheim-VCH.

71. Gupta, A.K. and M. Gupta, *Synthesis and surface engineering of iron oxide nanoparticles for biomedical applications.* Biomaterials, 2005. **26**(18): p. 3995-4021.

72. A.C.EWING, ed. *FOUNTAIN PEN COLLECT*. 1997, Running Press: Philadelphia, PA.

73. Piner, R.D., et al., *"Dip-pen" nanolithography.* Science, 1999. **283**(5402): p. 661-663.

74. Xie, X.N., et al., *Nanoscale materials patterning and engineering by atomic force microscopy nanolithography.* Materials Science & Engineering R-Reports, 2006. **54**(1-2): p. 1-48.

75. Hong, S.H. and C.A. Mirkin, *A nanoplotter with both parallel and serial writing capabilities.* Science, 2000. **288**(5472): p. 1808-1811.

76. Hong, S.H., J. Zhu, and C.A. Mirkin, *Multiple ink nanolithography: Toward a multiple-pen nano-plotter.* Science, 1999. **286**(5439): p. 523-525.

77. Weinberger, D.A., et al., *Combinatorial generation and analysis of nanometer- and micrometer-scale silicon features via "dip-pen" nanolithography and wet chemical etching.* Advanced Materials, 2000. **12**(21): p. 1600-+.

78. Zhang, H., S.W. Chung, and C.A. Mirkin, *Fabrication of sub-50-nm solid-state nanostructures on the basis of dip-pen nanolithography.* Nano Letters, 2003. **3**(1): p. 43-45.

79. Zhang, H., Z. Li, and C.A. Mirkin, *Dip-pen nanolithography-based methodology for preparing arrays of nanostructures functionalized with oligonucleotides.* Advanced Materials, 2002. **14**(20): p. 1472-+.

80. Lim, J.H. and C.A. Mirkin, *Electrostatically driven dip-pen nanolithography of conducting polymers.* Advanced Materials, 2002. **14**(20): p. 1474-+.

81. Maynor, B.W., et al., *Direct-writing of polymer nanostructures: Poly(thiophene) nanowires on semiconducting and insulating surfaces.* Journal of the American Chemical Society, 2002. **124**(4): p. 522-523.

82. Noy, A., et al., *Fabrication of luminescent nanostructures and polymer nanowires using dip-pen nanolithography.* Nano Letters, 2002. **2**(2): p. 109-112.

83. Demers, L.M., et al., *Direct patterning of modified oligonucleotides on metals and insulators by dip-pen nanolithography.* Science, 2002. **296**(5574): p. 1836-1838.

84. Wilson, D.L., et al., *Surface organization and nanopatterning of collagen by dip-pen nanolithography.* Proceedings of the National Academy of Sciences of the United States of America, 2001. **98**(24): p. 13660-13664.

85. Ben Ali, M., et al., *Atomic force microscope tip nanoprinting of gold nanoclusters.* Langmuir, 2002. **18**(3): p. 872-876.

86. Garno, J.C., et al., *Precise positioning of nanoparticles on surfaces using scanning probe lithography.* Nano Letters, 2003. **3**(3): p. 389-395.

87. Liao, J.H., L. Huang, and N. Gu, *Fabrication of nanoparticle pattern through atomic force microscopy tip-induced deposition on modified silicon surfaces.* Chinese Physics Letters, 2002. **19**(1): p. 134-136.

88. Li, Y., B.W. Maynor, and J. Liu, *Electrochemical AFM "dip-pen" nanolithography.* Journal of the American Chemical Society, 2001. **123**(9): p. 2105-2106.

89. Porter, L.A., et al., *Electroless nanoparticle film deposition compatible with photolithography, microcontact printing, and dip-pen nanolithography patterning technologies.* Nano Letters, 2002. **2**(12): p. 1369-1372.

90. Fu, L., et al., *Nanopatterning of "hard" magnetic nanostructures via dip-pen nanolithography and a sol-based ink.* Nano Letters, 2003. **3**(6): p. 757-760.

91. Su, M., S.Y. Li, and V.P. Dravid, *Miniaturized chemical multiplexed sensor array.* Journal of the American Chemical Society, 2003. **125**(33): p. 9930-9931.

92. Su, M., et al., *Moving beyond molecules: Patterning solid-state features via dip-pen nanolithography with sol-based inks.* Journal of the American Chemical Society, 2002. **124**(8): p. 1560-1561.

93. Ginger, D.S., H. Zhang, and C.A. Mirkin, *The evolution of dip-pen nanolithography.* Angewandte Chemie-International Edition, 2004. **43**(1): p. 30-45.

94. Jang, J.Y., et al., *Self-assembly of ink molecules in dip-pen nanolithography: A diffusion model.* Journal of Chemical Physics, 2001. **115**(6): p. 2721-2729.

95. Kumar, A., et al., *THE USE OF SELF-ASSEMBLED MONOLAYERS AND A SELECTIVE ETCH TO GENERATE PATTERNED GOLD FEATURES.* Journal of the American Chemical Society, 1992. **114**(23): p. 9188-9189.

96. Yan, L., X.M. Zhao, and G.M. Whitesides, *Patterning a preformed, reactive SAM using microcontact printing.* Journal of the American Chemical Society, 1998. **120**(24): p. 6179-6180.

97. Kim, Y. and C.M. Lieber, *MACHINING OXIDE THIN-FILMS WITH AN ATOMIC FORCE MICROSCOPE - PATTERN AND OBJECT FORMATION ON THE NANOMETER SCALE.* Science, 1992. **257**(5068): p. 375-377.

98. Muller, H.U., et al. *Nanostructuring of alkanethiols with ultrasharp field emitters*: Amer Inst Physics.

99. Ivanisevic, A., K.V. McCumber, and C.A. Mirkin, *Site-directed exchange studies with combinatorial libraries of nanostructures.* Journal of the American Chemical Society, 2002. **124**(40): p. 11997-12001.

100. Sheehan, P.E. and L.J. Whitman, *Thiol diffusion and the role of humidity in "dip pen nanolithography".* Physical Review Letters, 2002. **88**(15).

101. Maynor, B.W., Y. Li, and J. Liu, *Au "ink" for AFM "dip-pen" nanolithography.* Langmuir, 2001. **17**(9): p. 2575-2578.

102. Lee, K.B., et al., *Protein nanoarrays generated by dip-pen nanolithography.* Science, 2002. **295**(5560): p. 1702-1705.

103. Wei, L., et al., *Direct fabrication of protein arrays using dip-pen nanolithography.* Chemical Journal of Chinese Universities-Chinese, 2002. **23**(7): p. 1386-1388.

104. Ivanisevic, A. and C.A. Mirkin, *"Dip-Pen" nanolithography on semiconductor surfaces.* Journal of the American Chemical Society, 2001. **123**(32): p. 7887-7889.

105. Ivanisevic, A., et al., *Redox-controlled orthogonal assembly of charged nanostructures.* Journal of the American Chemical Society, 2001. **123**(49): p. 12424-12425.

106. Liu, X.G., S.W. Guo, and C.A. Mirkin, *Surface and site-specific ring-opening metathesis polymerization initiated by dip-pen nanolithography.* Angewandte Chemie-International Edition, 2003. **42**(39): p. 4785-4789.

107. Thomas, P.J., G.U. Kulkarni, and C.N.R. Rao, *Dip-pen lithography using aqueous metal nanocrystal dispersions.* Journal of Materials Chemistry, 2004. **14**(4): p. 625-628.

108. Gundiah, G., et al., *Dip-pen nanolithography with magnetic Fe2O3 nanocrystals.* Applied Physics Letters, 2004. **84**(26): p. 5341-5343.

109. Ding, L., et al., *Creation of cadmium sulfide nanostructures using AFM dip-pen nanolithography.* Journal of Physical Chemistry B, 2005. **109**(47): p. 22337-22340.

110. Lim, J.H., et al., *Direct-write dip-pen nanolithography of proteins on modified silicon oxide surfaces.* Angewandte Chemie-International Edition, 2003. **42**(20): p. 2309-2312.

111. Nam, J.M., et al., *Bioactive protein nanoarrays on nickel oxide surfaces formed by dip-pen nanolithography.* Angewandte Chemie-International Edition, 2004. **43**(10): p. 1246-1249.

112. Liu, X.G., et al., *Arrays of magnetic nanoparticles patterned via "dip-pen" nanolithography.* Advanced Materials, 2002. **14**(3): p. 231-+.

BIOGRAPHICAL INFORMATION

Jingwen He was born in Shanghai, China. She completed his Bachelor of Engineering in Polymer science and engineering from Shanghai University, Shanghai, China.

In fall 2007, she joined Materials Science and Engineering of the University of Texas at Arlington as a graduate student to obtain Master's Degree. She worked as a graduate research assistant in the Laboratory for two years and as teaching assistant in 2009 spring semester. After completion of Master's degree, she will look for an engineer position in materials-related areas.